



Open access

This is not the published version of the article / Þetta er ekki útgáfa greinarinnar

Author(s)/Höf.: Praise, S., Weisenberger, T. B., Cappelletti, P., Grimaldi, C., Rispoli, C., Jónasson, K., Jackson, M.D., Gudmundsson, M. T.

Title/Titill: Alteration progress within the Surtsey hydrothermal system, SW Iceland – A time-lapse petrographic study of cores drilled in 1979 and 2017

Year/Útgáfuár: 2020

Version/Útgáfa: Pre-print (óritrýnt handrit)

Please cite the original version:

Vinsamlega vísið til útgefnu greinarinnar:

Praise, S., Weisenberger, T. B., Cappelletti, P., Grimaldi, C., Rispoli, C., Jónasson, K., . . . Gudmundsson, M. T. (2020). Alteration progress within the Surtsey hydrothermal system, SW Iceland – A time-lapse petrographic study of cores drilled in 1979 and 2017. *Journal of Volcanology and Geothermal Research*, 392, 106754. doi:<https://doi.org/10.1016/j.jvolgeores.2019.106754>

Rights/Réttur: © 2020 Elsevier Ltd. All rights reserved.

1 **Alteration progress within the Surtsey**
2 **hydrothermal system, SW Iceland – a time-lapse**
3 **petrographic study of cores drilled in 1979 and 2017**

4
5 Simon Prause^a

6 Tobias Björn Weisenberger^a

7 Piergiulio Cappelletti^b

8 Carla Grimaldi^b

9 Concetta Rispoli^b

10 Kristján Jónasson^c

11 Marie D. Jackson^d

12 Magnús Tumi Gudmundsson^e

13
14 ^aIceland GeoSurvey (ÍSOR), Reykjavík, Iceland

15 ^bDipartimento di Scienze della Terra, dell’Ambiente e delle Risorse (DiSTAR), Università degli
16 Studi di Napoli Federico II, Naples, Italy

17 ^cIcelandic Institute of Natural History (IINH), Garðabær, Iceland

18 ^dDepartment of Geology and Geophysics, University of Utah, Salt Lake City, USA

19 ^eNordvulk, Institute of Earth Sciences, University of Iceland, Reykjavík, Iceland

20
21 * corresponding author: email: simon.prause@isor.is, phone: +354 528 1629

22 *Manuscript prepared for submission to Journal of Volcanology and Geothermal Research*

23 **Abstract**

24 The evolution of hydrothermal alteration in glassy and variably palagonitized tuff, erupted as
25 tephra in 1963 – 1964 on Surtsey, an island built in the offshore extension of Iceland’s southeast rift
26 zone, is documented through a comparative petrographic study of samples from drill cores recovered in
27 1979 and 2017. Time-lapse alteration within the low-temperature meteoric to seawater dominated
28 hydrothermal system of the volcano is characterized in terms of secondary mineral contents, alteration
29 rates and alteration style with depth. Between 1979 and 2017 palagonitization and cementation by
30 secondary minerals has progressed into previously poorly altered parts of the system, leading to
31 increased consolidation of the basaltic tephra. Alteration rates range between $1.05 - 42.5 \mu\text{m}\cdot\text{yr}^{-1}$ for
32 palagonitization of glass and $0.4 - 8.33 \mu\text{m}\cdot\text{yr}^{-1}$ for pseudomorphic olivine replacement by clay minerals
33 over a temperature interval of $47 - 140^\circ\text{C}$. Five distinct zones of alteration style, distinguished through
34 alteration mineralogy, development of authigenic phases over time, as well as degree of alteration are
35 described. Alteration of basaltic tephra at Surtsey volcano is defined by an early stage of phillipsite and
36 clay mineral formation, followed by a later stage of analcime and tobermorite formation as well as
37 replacement of phillipsite below the water table in zone 2 between 65.4 and 138.4 m. Only minor
38 advancement of alteration is detected in zone 3 between 138.4 – 150.3 m depth, where the primary
39 tephra remains largely unpalagonitized and unconsolidated. In contrast, from 1979 to 2017 alteration
40 has increased between 150.3 – 177.8 m depth, in zone 4, leading to rapid and extensive glass and olivine
41 alteration. The quantification of these time-lapse hydrothermal alteration processes at Surtsey provides
42 an important reference for studies of the evolution of young oceanic islands hosting hydrothermal
43 systems.

44 **Keywords**

45 Surtsey volcano, ICDP, SUSTAIN, palagonitization, basaltic glass, hydrothermal alteration

46 **1 Introduction**

47 In active geothermal systems, hydrothermal fluid flow is known to cause changes in host rock
48 mineral content via fluid-rock interaction, through processes such as geochemical leaching, as well as
49 precipitation of secondary mineral phases from the equilibrating geothermal fluid. The formation of
50 secondary minerals is essentially dependent on time, temperature, pressure, initial rock composition,

dissolved aqueous species, pH, fluid-rock-ratio and porosity/permeability (Browne, 1978; Giggenbach, 1984; Henley et al., 1985; Pauly et al., 2011). Thus, the nature and quantitative composition of a hydrothermal system's secondary mineral assemblage at depth may be considered to be indicative of the physicochemical properties and history of both host rock and hydrothermal fluid (e.g. Weisenberger et al., 2009; Kousehlar et al., 2012; Spürgin et al., 2019). As the geothermal system undergoes change with time, these properties too will be subject to variation, thereby resulting in an altered chemistry of the hydrothermal fluid, as well as a shift in the stability of secondary minerals. The effects of time as well as chemical and thermal changes are therefore an important aspect to consider in the petrographic study of hydrothermal alteration.

Within systems containing fresh basaltic glass (sideromelane), heat and chemical interaction with circulating fluids may cause devitrification of the glass (Marshall, 1961; Crovisier et al., 2003), leading to the formation of a metastable alteration product called palagonite. Palagonite, first described in 1845 by Sartorius von Waltershausen, occurs as a yellow to dark reddish brown amorphous to cryptocrystalline gel-like phase, commonly found as a surface alteration product of sideromelane, which can fully replace the original basaltic glass at advanced stages of the reaction. Palagonitization is recognized as a key factor in the lithification of loose vitric basalt tephra, fortifying volcanic edifices against erosion and increasing slope stability (Schiffman et al., 2006; Frolova, 2010; Romagnoli and Jakobsson, 2015), as well as being of global importance for oceanic crust-seawater chemical budgets (Staudigel and Hart, 1983; Walton et al., 2005; Pauly et al., 2011; Gernon et al., 2016). Additionally, the formation of palagonite and associated authigenic mineral assemblages from sideromelane is widely considered as a natural counterpart to alteration processes that may take place in radioactive waste storage borosilicate glasses, making the study of basaltic glass alteration relevant for the assessment of challenges involved in the long-term storage of these hazardous materials (Techer et al., 2001; Crovisier et al., 2003; Parruzot et al., 2015). Despite this potential relevance, the mineralogical nature of palagonite and its formation mechanism remain subject of research. Generally, it is accepted today, that palagonite forms as a result of dissolution of sideromelane in conjunction with glass hydration, which is usually accompanied by the precipitation of diverse mineral assemblages (Stroncik and Schmincke, 2002; Crovisier et al., 2003; Drief and Schiffman, 2004; Pauly et al., 2011). In this process, mobile elements are released from the glass (Singer and Banin, 1990; Stroncik and Schmincke, 2001; Pauly et al., 2011) and eventually form secondary minerals, such as clay minerals, zeolites and carbonates (Nayudu, 1964; Fisher and Schmincke, 1984; Walton and Schiffman, 2003; Pauly et al., 2011). Immobile elements become passively enriched (Stroncik and Schmincke, 2001). Palagonite may thus be considered as a residual material, containing both amorphous and microcrystalline phases, that remains after selective dissolution of the initial basaltic parent glass (Thorseth et al., 1991; Drief and Schiffman, 2004). The process of glass alteration and palagonitization can occur both abiotically, through purely geochemical processes, and also through microbial activity (Thorseth et al., 1992; Staudigel et al., 2008; Pedersen et al., 2015; Türke et al., 2015).

88 Previous studies have shown that palagonitization rates are strongly dependent on temperature,
89 with the process proceeding more rapidly at higher temperatures (Furnes, 1975; Jakobsson, 1978;
90 Jakobsson and Moore, 1986; Singer and Banin, 1990). Other important factors that affect the process of
91 palagonitization are porosity and water-rock ratio, fluid chemistry (including dissolved species, salinity
92 and pH), fluid flow and original glass composition (Moore, 1966; Jakobsson and Moore, 1986; Stroncik
93 and Schmincke, 2002; Crovisier et al., 2003; Pauly et al., 2011). As a result, palagonite does not have a
94 single fixed composition, but rather its specific chemical composition and the type of secondary mineral
95 phases, that may form from it, are strongly dependent on the abovementioned parameters. For this
96 reason, the name “palagonite” is to be taken as a descriptive expression, which designates the product
97 of a specific alteration process, rather than being a strictly defined term for a chemically well constrained
98 phase, as it may describe both crystalline and amorphous material of varying composition (e.g. Staudigel
99 and Hart, 1983). In addition, palagonite is known to change its composition and structure as it ages due
100 to progressive devitrification and diffusive processes (Thorseth et al., 1991; Stroncik and Schmincke,
101 2001; Pauly et al., 2011). Due to the ambiguity of the term some authors, such as Honnorez (1978) have
102 opted to forego the word palagonite entirely, in favor of the broader designation of “palagonitized glass”.

103 Many previous investigations have focused on palagonitization in a relatively low-temperature
104 environment, with studies on hydrothermal palagonitization rates being less common. Since
105 palagonitization under non-hydrothermal diagenetic conditions tends to be a relatively slow process,
106 with estimated palagonitization rates typically ranging between a few $10^{-3} - 10^{-2}$ $\mu\text{m}\cdot\text{yr}^{-1}$ (Hekinian and
107 Hoffert, 1975; Walton and Schiffman, 2003; Pauly et al., 2011), many aspects of palagonitization and
108 the evolution of the resulting secondary mineral assemblages over time remain poorly understood. In
109 this regard, the volcanic island of Surtsey, with its low-temperature meteoric to seawater dominated
110 hydrothermal system, offers a unique opportunity to study palagonitization and its resulting authigenic
111 smectite/zeolite/tobermorite mineral assemblage over time. The hydrothermal system at Surtsey is
112 hypothesized to have initiated in response to heating by the basaltic intrusions that fed lava flows from
113 1964 to 1967 (Friedman and Williams, 1970; Jakobsson and Moore, 1982; 1986; Stefanson et al., 1985).
114 Since this time, the vitric basaltic tephra deposits have been undergoing progressive hydrothermal
115 alteration, through the diverse processes that produce palagonitization of basaltic glass and cementation
116 of the deposits by authigenic minerals (Fig. 1).

117 The first Surtsey drill core, SE-01, was retrieved in 1979 from the vicinity of the island’s
118 southeastern vent, *Surtur* (Fig. 2). Investigations of the 181 m long core by Jakobsson and Moore (1986)
119 indicate that palagonitization of Surtsey tephra deposits is influenced by hydrothermal processes and
120 varies with temperature. Below sea level alteration rims of smectitic clay mineral, mainly nontronite,
121 were found to form around olivine crystal fragments. The thicknesses of these rims, much like the
122 thicknesses of palagonitization rims on basaltic glass particles, were positively correlated with
123 temperature.

124 A 192 m long drill core, SE-02b, was recovered at about 7 m lateral distance from SE-01 (Fig.
125 2) by the International Continental Scientific Drilling Program (ICDP) SUSTAIN project in 2017

126 (Jackson et al., 2019a; Weisenberger et al., 2019). The new core will allow us to build upon the prior
127 research by Jakobsson and Moore (1986) to investigate how alteration of basaltic tephra in a low-
128 temperature, hydrothermal system varies as a function of time, depth and temperature. For this purpose,
129 the archived 1979 Surtsey drill core is revisited for petrographic analysis and a comparison is made with
130 observations from corresponding depths of the 2017 drill core. The goal of this study is to evaluate and
131 quantify changes in secondary mineralization, palagonitization and lithification of the Surtsey tephra, to
132 characterize time-lapse alteration and constrain alteration rates. The petrographic results obtained from
133 this study form the groundwork for future geochemical investigations of the Surtsey drill cores.

134 2 Geological setting

135 Surtsey is the youngest and southernmost member of the Vestmannaeyjar archipelago, which
136 marks the seaward extension of Iceland's East Volcanic Zone (Moore, 1985; Jackson et al., 2015;
137 Schipper et al., 2016) (Fig. 2). First emerging from the ocean surface on November 15, 1963, Surtsey
138 was subsequently built up until June 5, 1967 by an interplay of early stage phreatomagmatic and mid to
139 late stage effusive volcanism (Jakobsson and Moore, 1982). The eruption that formed the island took
140 place in several episodes along a 4.5 km long ENE-trending array of five NNE-trending short submarine
141 volcanic fissures approximately 33 km off Iceland's southern coast (Thorarinsson et al., 1964; Moore,
142 1985). Two smaller edifices, *Syrtlingur* and *Jólnir* developed, but were subsequently eroded (Jakobsson
143 and Moore, 1982; Moore, 1985). Another volcanic ridge, *Surtla*, formed on the seafloor, between late
144 December 1963 and early January 1964, but did not grow large enough to rise above sea level. On
145 Surtsey an estimated amount of 0.7 – 0.8 km³ of very poorly sorted, alkali-basaltic, glassy tephra was
146 emplaced as bedded air fall and base surge deposits primarily via explosive discharge (cock's tails) and
147 continuous uprush (tephra fingers) (Thorarinsson, 1965; Jakobsson and Moore, 1982). These deposits
148 make up 60 – 70 vol.% of all erupted material on Surtsey with the remaining fraction composed of
149 crystalline alkali basalt, reworked sediments and sand/ tephra layers at depths ≥118.5 m below sea level
150 (Lorenz, 1974; Jakobsson and Moore, 1982).

151 One year after the cessation of volcanic activity, the first signs of an incipient hydrothermal
152 system were observed in the form of visible steam rising from the tephra pile and a zone of anomalous
153 heat exchange (Friedman and Williams, 1970). The nature of hydrothermal processes on the island and
154 associated alteration of the tephra deposits have been subject to earlier detailed studies (e.g. Jakobsson,
155 1972, 1978; Jakobsson and Moore, 1986; Jakobsson et al., 2000). In 1969, the first signs of
156 palagonitization of the basaltic glass fraction of the tephra became evident and by 1976 most tephra
157 within the thermal zone had undergone palagonitization (Jakobsson, 1971, 1972, 1978). Hydrothermal
158 alteration of vitric basaltic tephra by palagonitization together with the formation of natural secondary
159 mineral cements, have been recognized as key factors to the island's resistance to erosion, by causing
160 the lithification of the tephra deposits (Jakobsson et al., 2000; Jackson et al., 2015; Romagnoli and

161 Jakobsson, 2015). In addition, Surtsey has been recognized as having a secondary mineral assemblage
162 that is unique in both the Vestmannaeyjar archipelago as well as in greater Iceland (Jakobsson and
163 Moore, 1986; Jackson et al., 2019b).

164 3 The Surtsey hydrothermal system

165 The hydrothermal system at Surtsey is characterized by several distinct hydrological zones. The
166 uppermost zone above the water table is dominated by meteoric fluids that are derived from rainwater.
167 Surface vapors indicate that this depth interval contains steam zones.

168 The water table, which is influenced by tidal fluctuations, is located at ca. 58 m measured depth
169 for the two studied drill cores (Weisenberger et al., 2019). Geophysical borehole logging conducted
170 after drilling of SE-02b indicates a freshwater lens at this depth (Jackson et al., 2019a; Weisenberger et
171 al., 2019). The exact thickness of the lens remains unclear since fluids in the borehole were still disturbed
172 due to drilling when the measurements were conducted. The freshwater lens overlies more saline fluids
173 of modified seawater composition (Jackson et al., 2019a).

174 Temperature profiles obtained over the course of 37 years show, that the system has gradually
175 undergone cooling (Fig. 3). The system's temperature maximum occurs at a vertical depth of about 105
176 – 110 m below the surface for the two vertical boreholes considered in this study. Temperature at this
177 depth has decreased from 141°C in 1980 to 124°C in 2019. The temperature logs indicate a cooling
178 point at a depth of about 145 m below the surface, which likely represents a cold inflow zone
179 (Weisenberger et al., 2019; Jackson et al., 2019a).

180 4 Methods and materials

181 4.1 Thin section petrography

182 Petrographic thin sections were prepared for samples from the archive of the SE-01 drill core,
183 stored in core boxes at ambient temperatures since 1979, and the SE-02b drill core. All SE-01 thin
184 sections as well as reference samples from the SE-02b core (see Weisenberger et al., 2019) were
185 prepared using yellow epoxy resin. An additional series of thin sections from the SE-02b core was
186 prepared from selected research samples using blue epoxy resin. All samples were soaked in epoxy resin
187 prior to polishing, due to the fragility and friable nature of the sample material. Heating the epoxy resin
188 above 50 °C was avoided in all thin sections in order to preserve temperature-sensitive hydration. Table
189 1 provides an overview of selected samples for this study.

190 Primary mineral phases and authigenic features, such as altered glass and secondary minerals,
191 were quantified by point counts, using a step interval of 0.18 mm. The number of counted points was
192 dependent on the individual sample and ranged from 603 to 4557 points, with an average number of
193 counts per sample of 2322. The degree of palagonitization was determined as the fraction of basaltic
194 glass (sideromelane) in a sample, which has become palagonitized, given as

$$195 \frac{V_{\text{palagonitized glass}}}{(V_{\text{palagonitized glass}} + V_{\text{glass}})} \cdot 100 \text{ vol. \%}$$

196 where $V_{\text{palagonitized glass}}$ and V_{glass} refer to the total volume of palagonitized glass and sideromelane
197 within a given thin section as indicated by point counts. Thicknesses of alteration rims (i.e. palagonitized
198 glass and clay mineral rims around olivine) were obtained by conducting as many measurements as
199 possible by use of a petrographic microscope followed by determination of median values for each
200 sample. Sideromelane was identified purely based on its distinct coloration as well as its optical isotropy
201 (complete extinction under cross-polarized light). However, as a recent study by Jackson et al. (2019b)
202 has demonstrated, such seemingly unaltered glasses may also contain nanocrystalline clay minerals,
203 which are unobservable under the microscope. Here we use the term “sideromelane” to refer to the
204 fraction of glassy lapilli, which appears unaltered based purely on optical microscopy.

205 4.2 X-ray powder diffraction

206 X-ray powder diffraction (XRPD) analysis was performed on samples of the 1979 core (SE-01)
207 in order to confirm the results of the point count data. XRD analyses were carried out using a Panalytical
208 X'Pert Pro diffractometer (RTMS X'Celerator detector) and Bruker D2 Phaser (LINKEYE detector)
209 diffractometer at the Department of Earth Sciences, Environment and Resources (DiSTAR) of the
210 University of Naples Federico II.

211 The following operative conditions were used: CuK α radiation, 40 kV, 40 mA, 29 range from 4
212 to 70°, equivalent step size 0.017° 29, 30 s per step counting time for X'Pert Pro; CuK α radiation, 30
213 kV, 15 mA, 29 range from 4 to 70°, 0.02 29 step size, 66 s per step counting time for Bruker D2 Phaser.
214 The analyses were used to obtain a calibration between the two different diffractometers. Each sample
215 was disaggregated by hand in an agate mortar to obtain a homogeneous powder (particle size <200 μm).
216 An amount of 20 wt.% corundum (α -Al₂O₃, Buehler micropolish, 1 μm grain size) was added as an
217 internal standard. This mixture was subsequently micronized (grain size <10 μm) by using a McCrone
218 Micronising Mill, with agate cylinders and 10 mL of deionized water for 15 min of grinding time. This
219 technique was used to reduce preferred orientation, primary extinction or crystallite size issues which
220 commonly affect clay minerals (Bish and Chipera, 1987). For the qualitative interpretations of XRPD
221 patterns the Panalytical HighScore Plus 3.0d software was used, while BRUKER TOPAS 5.0 software
222 was employed for quantitative evaluations with the combined RIR/Rietveld approach.

223 4.3 Surtsey drill cores

224 Two drill cores have been selected for this study: SE-01 and SE-02b (Fig. 2). The studied drill
225 core samples, except for the samples obtained from crystalline basalt, can universally be described as
226 hypocristalline (lapilli-) tuff of inequigranular grain size distribution at different stages of
227 palagonitization, which contains varying amounts of secondary minerals associated with palagonitic
228 glass alteration. The principal constituents of the samples are angular to slightly rounded ash to lapilli-
229 sized fragments of sideromelane. The outline given below is only intended as a very brief overview of
230 macroscopic lithological characteristics. For a more comprehensive description of the 1979 and 2017
231 Surtsey drill cores the reader is referred to Jakobsson and Moore (1982) and Weisenberger et al. (2019).

232 4.3.1 SE-01

233 Above water level, the tuff is beige to brown in color and remains poorly altered. The degree of
234 consolidation is typically low. Some primary layering may be observed locally. At 55.3 m, which is
235 close to the uppermost tidal dominated water level, the first macroscopically visible signs of alteration
236 in the form of white mineral cements in pore space become apparent. These increase in abundance
237 downcore, leading to a progressive reduction of estimated pore space with depth as the rock begins to
238 take on a greenish hue and increases in hardness and density, as inferred by weight. Between 72.3 and
239 83.4 m a basaltic intrusion is present. The tuff is more poorly consolidated and friable in the zone
240 between ca. 139.3 – 150.3 m, locally leading to poor core recovery between 140.0 – 143.8 and 148.5 –
241 150.3 m. Below this depth, the material becomes slightly more consolidated up until 157.3 m. Below
242 157.3 m core recovery was again poor with the recovered tuff being dark gray in coloration as well as
243 very friable. Alteration mineralogy at this depth consists mainly of anhydrite, which occurs as a
244 macroscopically visible white to translucent phase in the pore space and along fractures. Between 170.5
245 and 180.1 m only cuttings were recovered.

246 4.3.2 SE-02b

247 Armored lapilli were locally described above water level as well as down to ca. 62.6 m depths
248 (Weisenberger et al., 2019). The basaltic intrusion found in SE-01 at 72.3 – 83.4 m depths is not present
249 in SE-02b, despite the horizontal distance between the cores being less than 7 m, possibly indicating a
250 complex geometry of the intrusive body. Unlike in SE-01, fully consolidated core material was
251 recovered from the area between 139.3 – 150.3 m and below 157.3 m. Despite this, the tuff remains
252 poorly altered in the depth interval between 138.4 – 150.3 m. Here the main secondary minerals are
253 anhydrite, gypsum and calcite, rather than zeolites or tobermorite, which dominate in the more strongly
254 altered zones. Estimated porosities (Table 1) for this poorly altered zone are high, reaching up to 38.6
255 vol.%. The tuff in the depth interval below 150 m down to 178 m is more consolidated and shows
256 extensive signs of alteration in the form of macroscopically visible cementation and darkened coloration
257 as well as palagonitization. Below 178 m the rock remains poorly altered and very friable.

258 5 Results

259 5.1 Primary phases

260 The primary crystalline phases present in the Surtsey tuff samples are plagioclase,
261 clinopyroxene and olivine. These occur as (micro-) phenocrysts in the glassy particles and as sand sized
262 crystal fragments. Minor amounts of opaque phases are present as well. A brief description of the
263 primary phases is given below.

264 5.1.1 Sideromelane

265 Sideromelane appears in thin section as a vesicular bright yellow to pink gel-like phase
266 containing sporadic phenocrysts of plagioclase, olivine and clinopyroxene. It is distinguished from
267 palagonitized glass mainly by its characteristic color, as opposed to the darker reddish brown of type I
268 palagonitization rims (see 5.2.1 Palagonitized glass). Furthermore, the complete optical isotropy of
269 sideromelane makes it distinct from type II and III palagonitized glass. Despite this seemingly obvious
270 distinction, it should be noted that “fresh” sideromelane is identified here under purely optical criteria
271 and thus some alteration of the glass may have occurred on a microscale. Since submicroscopic
272 nanocrystalline phases, such as clay minerals, as identified by Jackson et al. (2019b), cannot be
273 identified by optical microscopy, our definition of “sideromelane” cannot possibly account for their
274 presence.

275 5.1.2 Plagioclase

276 Plagioclase typically occurs in the form of anhedral, single crystals or granular aggregates with
277 an average grainsize between 150 – 200 µm, typically forming a microlitic texture within sideromelane.
278 Some rare larger phenocrysts of up to 1 cm can be found in the Surtsey lapilli-tuff. Both above and
279 below water level some of these larger massive phenocrysts show minor signs of dissolution in the form
280 of serrated or frayed grain boundaries and occasional low amounts of secondary clay mineral formation.
281 Smaller plagioclase microphenocrysts generally decrease in abundance within the temperature
282 maximum of the system at 105 – 110 m, leaving behind voids in glass upon their dissolution. According
283 to XRPD, the amount of plagioclase in the tuff lies between 2 – 19 wt.% with an average of 9 wt.%
284 (Grimaldi, 2018).

285 5.1.3 Clinopyroxene

286 Clinopyroxene is very common in the Surtsey tephra, making up a fraction between 2 – 9 wt.%
287 (average: 6 wt.%) of the phases identified in the tuff samples by XRPD (Grimaldi, 2018). It occurs in
288 the form of anhedral granular to columnar microphenocrysts in sideromelane. These typically have an
289 average size of about 230 µm.

290 5.1.4 Olivine

291 Olivine commonly occurs as granular, massive and rarely prismatic anhedral to subhedral
292 crystals. Very few euhedral crystals are present. Below water level olivine crystals are commonly
293 rimmed by authigenic clay minerals. Within the zone of maximum temperature at 105 – 110 m
294 (Weisenberger et al., 2019) unaltered olivine is uncommon and most crystals are altered to
295 nanocrystalline clay mineral. At this depth, fresh unaltered olivine, as determined by XRPD, forms 0 –
296 3 wt.% (average: 1 wt.%) of the lapilli tuff (Grimaldi, 2018). Crystal size typically ranges between 200
297 – 600 µm, with some larger phenocrysts reaching up to 3 mm in diameter. The thickness of the alteration
298 rims on olivine, much like that of the palagonitized glass rims, is positively correlated with temperature
299 and has noticeably increased between 1979 and 2017 in samples from corresponding depths (Fig. 4).

300 5.2 Authigenic alteration phases

301 Alteration in both Surtsey drill cores is dominated by palagonitization of sideromelane and the
302 formation of phillipsite, analcime as well as acicular tobermorite. Other secondary phases include clay
303 minerals, which occur either as highly birefringent microcrystalline mineral aggregates in altered glass
304 or as replacement rims on olivine, calcium sulphates (anhydrite, gypsum and bassanite), and calcite.

305 5.2.1 Palagonitized glass

306 Based on petrographic investigations of lapilli-sized fragments in thin sections of the archived
307 1979 Surtsey SE-01 drill core and the 2017 SE-02b drill core, we distinguish three principal types of
308 palagonitic textures.

309 5.2.1.1 *Type I (gel-palagonite)*

310 The altered glass falling into this category is clear, translucent and reddish brown in coloration
311 (Fig. 5A). Its appearance is gel-like and amorphous to slightly crystalline (e.g. Stroncik and Schminke,
312 2001, 2002). This type of palagonite commonly marks zones, where the degree of palagonitization is
313 ≤80.0 vol.%. Type I palagonitization rims are comparatively thin as well as optically isotropic.

314 5.2.1.2 *Type II (fibro-palagonite)*

315 Type II altered glass (Fig. 5B) rims possess a grainy to fibrous texture. In plane polarized light
316 they are reminiscent of type I rims, yet they may be slightly brighter in appearance. Rims belonging to
317 this category are cryptocrystalline and show strong birefringence with colorful yellow, green and red
318 interference colors, which strongly resemble those of clay minerals – a property, which sets them apart
319 from type I palagonitized glass rims. Type II occurs in depth intervals of intermediate temperature.
320 Between 1979 and 2017 type II has replaced type I at the lower end of the temperature spectrum and in
321 turn has become replaced by type III palagonitized glass rims in depth intervals of comparatively higher
322 temperatures.

323 5.2.1.3 Type III

324 Type III altered glass (Fig. 5C) occurs below water level in both drill cores. It is darkened,
325 opaque and spotty rather than translucent in appearance. Interference colors are far less intense than in
326 type II and in some instances the material might appear completely opaque under cross polarized light.
327 In SE-01 this kind of palagonitization is only found close to the hydrothermal system's zone of
328 maximum temperature. In SE-02b it has spread both upwards and downwards to become the dominant
329 type of palagonitized glass between 67.5 – 134.3 m as well as being present together with type II below
330 153.3 m.

331 In instances, where different types appear together, most prominently in SE-02b between 150.3
332 – 177.8 m, they are generally concentrically arranged around sideromelane in the order of type III →
333 type II → type I → sideromelane (Fig. 6).

334 5.2.2 Analcime

335 Analcime (general formula: $\text{NaAlSi}_2\text{O}_6 \cdot (\text{H}_2\text{O})$) is the most abundant secondary mineral phase
336 in terms of both volume and weight percentages according to XRPD and point counts in most of the
337 samples. The mineral is typically present as colorless surface textures of massive habit inside the inner
338 walls of cavities, identifiable under crossed polarizers due to its optical isotropy (Fig. 7a). The relative
339 abundance of analcime is positively correlated with both temperature and the degree of palagonitization.
340 The amount of analcime is found to generally have increased in samples from nearly all depths from
341 1979 to 2017.

342 5.2.3 Clay minerals

343 A variety of clay minerals, identified through XRPD (Grimaldi, 2018) as consisting of
344 nontronite, montmorillonite and vermiculite, are present within all tuff samples investigated in this
345 study. Granular to platy mineral aggregates displaying high interference colors are commonly found in
346 available pore space. Clay minerals also occur in the form of alteration rims around olivine phenocrysts.
347 Lastly, submicroscopic to microscopic clay minerals appear as replacement product of sideromelane in
348 palagonitized glass. XRPD does not allow for discrimination between different clay mineral species at
349 their distinct structural positions. The abovementioned highly birefringent dark brown cryptocrystalline
350 clay mineral rims on olivine grains (Fig. 7b, c) are observed exclusively below water level. Above water
351 level olivine typically appears unaltered under the microscope in both SE-01 and SE-02b. The thickness
352 of the olivine alteration rims is positively correlated with temperature. The rims are not observed in
353 samples from the poorly altered zones in the cores between ca. 138 – 150 m, as well as from the very
354 bottom of both drill holes below 159 m in SE-01 and 178 m in SE-02b respectively.

355 5.2.4 Tobermorite

356 Tobermorite (general formula: $\text{Ca}_5\text{Si}_6\text{O}_{16}(\text{OH}_2)\cdot 7\text{H}_2\text{O}$) is present as colorless acicular crystals,
357 arranged as either discrete needles or sheaf like bundles (Jakobsson and Moore, 1986) (Fig. 7d). It
358 commonly forms within cavities and is frequently associated with analcime as well as phillipsite in some
359 samples, particularly below water level (Fig. 8b).

360 5.2.5 Phillipsite

361 In thin section phillipsite (general formula: $(\text{K},\text{Na},\text{Ca})_{1-2}(\text{Si},\text{Al})_8\text{O}_{16}\cdot 6\text{H}_2\text{O}$) occurs as colorless
362 intergrowing prismatic crystals often radiating from a common point of origin. Under crossed polarizers
363 it is distinguishable by its low interference colors (grey I) (Fig. 7e). It commonly fills smaller (50 – 200
364 μm) pores and, unlike analcime, only rarely occurs as surface textures in larger cavities. Phillipsite
365 concentrations in the tuff samples appear to have decreased in the higher temperature zones, most likely
366 due to dissolution and/ or replacement by other phases (Figs. 7f, 8). Samples that are particularly high
367 in phillipsite are generally marked by a low degree of palagonitization and occasionally by the presence
368 of type I palagonitized glass.

369 5.2.6 Calcite

370 Calcite occurs infrequently above and below water level. In more shallow depths, calcite is
371 present as small ($\leq 10 \mu\text{m}$) massive to prismatic grains displaying characteristically high interference
372 colors. Calcite crystals below water level are frequently larger than their counterparts above water level.
373 In SE-02b between 140 – 150 m, several samples show particularly high calcite contents (Fig. 7g).

374 5.2.7 Calcium sulphate minerals

375 Anhydrite (CaSO_4) and gypsum ($\text{CaSO}_4\cdot 2\text{H}_2\text{O}$) are generally present in trace amounts in most
376 samples. Anhydrite occurs as granular to prismatic crystals $\leq 10 \mu\text{m}$ in size, which appear to have
377 precipitated after tobermorite as a result of late stage hydrothermal alteration. Samples from the poorly
378 altered portion of the cores between ~138 – 150 m and from the bottom of the drill holes contain larger
379 prismatic or, more rarely, massive anhydrite crystals (Fig. 7h) in pore space or as fillings within
380 fractures.

381 Only traces of gypsum were detected in the XRPD diffraction measurements of SE-01 samples.
382 In SE-02b gypsum is observed under the microscope above water level at 31.2 m and 40.4 m as well as
383 in the poorly altered zone at 144.1 m and near the bottom of the core around 180 m, where it can be
384 found either by itself as massive, tabular or amygdaloidal crystals or together with prismatic anhydrite
385 (Fig. 7i). XRPD diffraction also identified bassanite ($\text{CaSO}_4\cdot 0.5\text{H}_2\text{O}$) in the sample from 169.5 m depth
386 in SE-01.

387 5.3 Alteration in archived 1979 SE-01 drill core samples

388 5.3.1 Palagonitized glass

389 Above water level, the degree of palagonitization is between 73.3 – 82.4 vol.%, except for the
390 sample from 43.6 m, which is only 21.6 vol.% palagonitized. The most common type of palagonitized
391 glass at these depths is the optically isotropic, presumably amorphous type I, or gel-palagonite. All
392 samples above 65.4 m depth are relatively high in X-ray amorphous contents (generally around 60 – 70
393 wt.%). At 55.8 m, palagonitized glass rim thickness, as well as palagonitization extent begins to rapidly
394 increase with depth. Despite the degree of palagonitization being 95.5 – 100.0 vol.% at almost all depths
395 from 65.4 – 120.6 m, a poorly palagonitized layer exists around 95.4 m, in which nearly half of the
396 sideromelane remains unaltered. This layer is darker and finer grained compared to surrounding tuff and
397 exhibits very low porosities. It forms a sharp border with the underlying tuff at 95.5 m, which exhibits
398 higher porosity and a very high degree of palagonitization of >95.0 vol.% (Table 1). Between 55.8 –
399 105.0 m, 120.6 – 137.8 m and 150.3 – 156.9 m, type II palagonitized glass (fibro-palagonite) is generally
400 the most abundant form of palagonitized glass. The amount of X-ray amorphous contents for these
401 samples is normally below 60 wt.% – except for the two samples from 55.8 and 65.4 m (Grimaldi, 2018).
402 Only the three samples retrieved from 105.0 m, 111.0 m and 120.6 m, the first two of which correspond
403 to the zone of maximum temperature, contain type III palagonitized glass. X-ray amorphous contents
404 are highest at 105.0 m, at 85 wt.%. Samples from the depth interval between 137.8 – 150.3 m generally
405 show either very little palagonitization or the glass appears entirely unaltered under the petrographic
406 microscope. The amount of X-ray amorphous phases for these samples is 68 – 70 wt.%. Only type I
407 rims with a median diameter of 40 µm are present at 148.3 m. The sharp lower boundary of this interval
408 is visible at the macro- and microscopic scales. The rock turns from a greyish, friable, poorly
409 consolidated and mostly unpalagonitized lapilli-tuff to a more well consolidated, slightly palagonitized
410 lapilli-tuff that contains thin type II palagonitized glass rims, ranging between 20 – 90 µm. This change
411 is not gradual but abrupt, occurring over just a few µm in the thin section of the sample from 150.3 m.
412 The transition is accompanied by a decrease in the X-ray amorphous content from 68 wt.% in the
413 unpalagonitized upper half of this sample to 59 wt.% in the slightly palagonitized lower half. The degree
414 of palagonitization slightly increases with depth between 150.3 and 156.9 m. Below 156.9 m no
415 palagonitized glass rims are detected under the microscope. However, nano-analytical techniques may
416 reveal minor alteration features on a submicroscopic scale at these depths (Jackson et al., 2019b).

417 5.3.2 Clay Minerals

418 Clay minerals are found throughout most of the samples in SE-01, as microcrystalline highly
419 birefringent granular to platy mineral aggregates in pore space and as microscopic to submicroscopic
420 granular particles in palagonitized glass. At 72.4 m clay minerals also begin to appear as rims on olivine
421 grains as a pseudomorphic alteration phase (Fig. 7b). The thickness of these rims ranges from 20 – 95
422 µm and varies as a function of temperature. In some instances, olivine has become entirely replaced by

423 secondary clay minerals (Fig. 7c). Olivine rims are not observed under the microscope in samples from
424 the interval between 140.0 – 150.3 m. Below this depth interval, only 20 µm thin rims are observed in
425 the sample from 156.9 m.

426 5.3.3 Phillipsite

427 Phillipsite contents are higher than analcime in some samples above water level (Table 1, Fig.
428 9). Particularly high amounts of phillipsite are found in the tuff at 22.0 m, which contains 5.5 vol.%
429 (point counts)/ 11 wt.% (XRPD) of this mineral, as opposed to only about 4.1 vol.%/ 7 wt.% analcime.
430 Below water level, the amount of phillipsite begins to decrease with depth and remains generally low
431 above 137.8 m. Several phillipsite grains show signs of dissolution and replacement by analcime and
432 tobermorite (Fig. 8). The samples from 137.8 m, 148.3 m and 150.3 m are enriched in phillipsite
433 compared to other samples below water level. These samples contain significantly more phillipsite than
434 analcime, which is unusual below water level.

435 5.3.4 Analcime

436 Analcime shows a positive correlation with both degree of palagonitization and temperature. Its
437 contents strongly increase below water level and reach peak amounts of up to 26 wt.% according to
438 XRPD between 95.5 – 111.0 m, which roughly coincides with the area of maximum temperature in the
439 system. The top and bottom borders of the poorly altered and very friable interval spanning the area
440 below 137.8 m, down to 150.3 m contain very little to no analcime and are instead dominated by
441 phillipsite (see above). Much like phillipsite and tobermorite, analcime is not observed in any relevant
442 quantities below 157.3 m depths, where consolidation of the tuff and the degree of palagonitization
443 remain exceedingly low.

444 5.3.5 Tobermorite

445 Thin section petrography and XRPD identified very little to no (typically <1 wt.%/ vol.%)
446 tobermorite in SE-01 above water level. Below water level tobermorite is weakly correlated with
447 temperature and the degree of palagonitization. Similar to analcime, tobermorite reaches its maximum
448 concentrations in the samples around the area of highest temperature between 95.4 – 111.0 m, with the
449 exception of a narrow zone around 95.6 m where the rock is intersected by a series of discrete fractures
450 filled with calcium sulphate mineral phases, identified as anhydrite in thin section, as well as possibly
451 minor amounts of gypsum according to XRPD. This specific sample contains virtually no tobermorite,
452 despite originating from the general area of highest tobermorite concentrations. Tobermorite is only
453 detected in traces via XRPD in the seemingly unpalagonitized sample from 169.5 m and not observed
454 at all in the corresponding thin section.

455 5.3.6 Calcium sulphate minerals

456 Calcium sulphates occur throughout the samples from SE-01. Many samples, especially above
457 water level, contain small ($\leq 10 \mu\text{m}$) prismatic to granular anhydrite often associated with tobermorite.
458 Enrichment in anhydrite, resulting in the formation of larger prismatic crystals of ca. 200 – 700 μm
459 length, occurs in several samples below water level. Examples for this include the lower contact between
460 the basaltic intrusion and the tuff at 83.5 m, 95.6 m, where anhydrite occurs as filling in fractures, 105.0
461 m, 150.3 m, and especially 169.5 m, where anhydrite is strongly enriched in the otherwise seemingly
462 unaltered vitric tuff of this depth.

463 While anhydrite is the only calcium sulphate phase identified in thin section, XRPD also detects
464 gypsum and bassanite. Gypsum occurs mostly in traces in several samples throughout the core and
465 potentially in larger quantities below the basaltic intrusion at 83.5 m, though this is not observed in the
466 thin section sample. Bassanite is detected only at 169.5 m, with increased anhydrite content.

467 5.3.7 Calcite

468 Minor amounts of massive to prismatic calcite are scattered throughout the tuff of the 1979 core.
469 Individual crystals are typically $\leq 10 \mu\text{m}$ in diameter and appear to have formed after analcime and
470 tobermorite above water level and before or simultaneous with analcime below water level. No
471 particular patterns or enrichments for this mineral are observed in SE-01.

472 5.4 Alteration in 2017 SE-02b drill core samples

473 5.4.1 Palagonitized glass

474 Samples from the uppermost section of the system situated above the tidally influenced water
475 level, are not fully palagonitized. Rather, the degree of palagonitization remains relatively steady
476 between 22.6 – 56.0 m at around 82.0 vol.% (Table 1, Fig. 4). Type I palagonitic textures are prevalent
477 in this part of the system but have locally been replaced by the more crystalline and highly birefringent
478 type II rims at 31.2 m and below. The degree of palagonitization is ≥ 90.0 vol.% for all samples between
479 water level and 141.5 m. The tuff between 141.5 m and 147.1 m remains only weakly palagonitized.
480 Type III palagonitic textures are far more widespread below water level than in SE-01 and dominate in
481 samples between 67.5 to 134.3 m. SE-02b samples corresponding in depth to the weakly altered and
482 poorly consolidated interval between 157.5 – 177.8 m in SE-01 are nearly completely palagonitized. A
483 concentric arrangement of palagonitized glass rims in the form type III → type II → type I →
484 sideromelane is very common below 150.3 m.

485 5.4.2 Clay minerals

486 The distribution of clay minerals in SE-02b is the same as in SE-01. Both granular to platy
487 aggregates in pore space and microscopic to submicroscopic particles in palagonitized glass are

488 common. In SE-02b the first signs of olivine alteration to clay minerals are detected at 62.1 m, slightly
489 below the water table in the borehole (~58 m, Weisenberger et al., 2019). Olivine alteration rims show
490 greater diameters in samples from SE-02b, when compared to depth-equivalent samples from SE-01
491 (Fig. 4). No alteration rims are observed along olivine grains within samples between 141.5 – 150.3 m
492 or in the bottom section of the drill core below 177.8 m where no palagonitization has been detected
493 from our petrographic analysis. However, thin olivine rims about 20 – 45 µm in thickness are generally
494 found in between these depth intervals at 157.5 – 177.8 m.

495 5.4.3 Phillipsite

496 Samples from the uppermost 62.1 m of SE-02b contain more phillipsite than samples at
497 corresponding depths in SE-01. The greatest enrichment of phillipsite in SE-02b is found around 43.7
498 m, where the tuff remains slightly altered and only poorly palagonitized in SE-01, but the overall extent
499 of alteration is much greater in SE-02b. Consistently lower amounts of phillipsite are present from 65.4
500 to 138.4 m in SE-02b as compared to SE-01 (Table 1, Fig. 9). Phillipsite dissolution and replacement
501 by analcime and tobermorite is observed throughout most of the samples, even at depths where
502 phillipsite has increased since 1979. The phillipsite-rich upper and lower borders of the poorly altered
503 depth interval, located in SE-01 between 137.8 – 150.3 m show increased phillipsite contents in SE-02b
504 as well, although the upper zone of enrichment is found at a slightly greater depth at 141.5 m in the 2017
505 core. The lower phillipsite enriched zone is found at 150.3 m, at the same measured depth where it was
506 detected in SE-01.

507 5.4.4 Analcime

508 Similar to SE-01, analcime contents are positively correlated with temperature and the degree
509 of palagonitization in SE-02b. The amount of analcime has increased from 1979 to 2017 at almost all
510 depths and is highest at 92.6 – 101.5 m, where it has about doubled. As is the case with phillipsite and
511 tobermorite, secondary analcime mineralization has extended into previously weakly altered tuff
512 between 157.5 – 177.8 m.

513 5.4.5 Tobermorite

514 Point counts of thin sections at 43.6 m and above indicate significantly higher tobermorite
515 content than their SE-01 counterparts, which contain almost no tobermorite (Table 1). In these samples,
516 tobermorite is frequently associated with other Ca-bearing phases such as plagioclase, clay minerals or
517 gypsum. Particularly the sample at 34.8 m containing 9.3 vol.% tobermorite exhibits some of the highest
518 concentrations of this mineral observed in any of the studied samples from either drill core. In the hottest
519 areas of the system tobermorite contents are found to be lower in SE-02b than in SE-01, with the samples
520 between 86.5 and 101.5 m all showing less tobermorite than the samples from SE-01 from comparable
521 depths. Two distinct peaks in tobermorite content are found in the samples at 138.4 and 148.7 m, at
522 depths where previously only phillipsite had been enriched, but little to no increase in tobermorite or

523 analcime content was detected in the 1979 samples. The highest concentrations of tobermorite of 14.3
524 vol.% are present in the sample from 177.8 m, which is situated close to the very bottom of the
525 palagonitized area in SE-02b.

526 5.4.6 Calcium sulphate minerals

527 The poorly altered zone contains high quantities of calcium sulphate phases. Gypsum, which in
528 SE-01 is only identified via XRPD, but not observed in thin section is abundant and observable under
529 the microscope in SE-02b at 144.1 m. It typically either occurs alone or around prismatic anhydrite, with
530 which it is frequently associated. Larger gypsum crystals are also found at 31.2 m and 40.4 m in the
531 meteoric part of the system. In these samples, gypsum seems to become partially replaced by
532 tobermorite. Anhydrite and gypsum are the most common alteration minerals below 177.8 m, where no
533 palagonitization is observed under the microscope in the 2017 drill core.

534 5.4.7 Calcite

535 Calcite is primarily found in larger amounts together with gypsum and anhydrite between 141.5
536 – 150.3 m. There, it forms massive, up to 400 µm large crystals (Fig. 7g) filling smaller vesicles or
537 growing on the inside of larger fractures. Smaller amounts of calcite are especially found above water
538 level, where all samples contain at least some traces of this mineral. Very little to no calcite occurs in
539 the bottom part of the hole, where gypsum and anhydrite, the phases it is otherwise often associated
540 with, are very common.

541 5.5 Alteration sequence and changes in secondary mineralogy

542 Two authigenic zeolite species, phillipsite and analcime, have been identified. Chabazite as
543 described by Jakobsson and Moore (1986) for the upper 0 – 4 m of the SE-01 drill core, is not reported
544 here, most likely owing to the fact that the most shallow samples in this study were from 4.9 m and 13.2
545 m for SE-01 and SE-02b respectively, which is below the documented depth range for this zeolite phase.
546 Analcime is positively correlated with temperature and the degree of palagonitization. Phillipsite is more
547 abundant in samples that show a lower extent of glass alteration overall, and comparatively lower
548 amounts of analcime and tobermorite. Examples include the samples from 22.0, 137.8, 148.3 and 150.3
549 m depths in SE-01 and from 43.7, 141.5 and 150.3 m depths in SE-02b (Table 1, Fig. 9). Point count
550 data confirms a net loss of phillipsite at 65.4 – 138.4 m between 1979 and 2017. Thin section
551 petrography indicates that this may be due to dissolution of phillipsite as well as alteration to other
552 phases, such as analcime. Thus, phillipsite may form as an earlier alteration product when compared to
553 analcime both above and below the water table and become lost – at least below water level – due to
554 dissolution as glass alteration progresses and the compositions of interstitial fluids change. The amount
555 of phillipsite has either remained the same or increased in samples below approximately 150 m, where
556 little alteration was observed in SE-01. Increased alteration rates of palagonitized glass and olivine rims

557 are estimated for the SE-02b drill core samples at this depth interval (see 6.3.1 Alteration rates in zone
558 4). Tobermorite overgrows analcime or occurs alongside of it on the inner walls of pores and fractures.
559 In contrast, analcime is rarely found overgrowing tobermorite. While gypsum is only detected via XRPD
560 and not observed in thin section for the SE-01 sample set, several thin section samples from SE-02b –
561 particularly between 142.6 – 147.1 m and below 177.8 m – are found to contain gypsum. Gypsum is
562 therefore interpreted as having formed relatively late, as opposed to anhydrite which is already present
563 in relevant quantities in the 1979 samples (Table 1).

564 **6 Discussion**

565 **6.1 Time-lapse alteration with depth**

566 Tephra alteration in Surtsey's hydrothermal system changes as a function of time and depth. We
567 identify five zones of distinct alteration behavior observable in both the 1979 and 2017 drill cores. An
568 overview of the zones and associated changes in alteration behavior is given in Figure 10. The alteration
569 zones are defined as follows:

570 **6.1.1 Zone 1 (upper palagonitization zone)**

571 In zone 1, situated above 65.4 m in SE-01 and 58.9 m in SE-02b, palagonitization progresses
572 slowly, when compared to the remaining palagonitized parts of the system. No olivine alteration is
573 observed. Phillipsite contents are locally higher than analcime contents, especially in less palagonitized
574 samples, and have either increased or remained steady between 1979 and 2017. Zone 1 persists slightly
575 below water level, which lies around 58 m depth.

576 **6.1.2 Zone 2 (middle palagonitization zone)**

577 Below zone 1, secondary clay mineral rims begin to form around individual olivine grains,
578 eventually leading to complete pseudomorphic replacement. The onset of this alteration marks the
579 beginning of zone 2, reaching down from the bottom border of zone 1 to 137.8 m in SE-01 and 138.4 m
580 in SE-02b. At the transition between zones 1 and 2 palagonitization rim thicknesses suddenly increase
581 by two to four times, resulting in a strong increase in the degree of palagonitization (Fig. 4). This increase
582 is observed in both cores. The most common type of palagonitic rim in zone 2 is type II in SE-01, which
583 has evolved to type III in SE-02b, reflecting a more rapid palagonite maturation in zone 2 as compared
584 to zone 1. Alteration degree and thus rim thicknesses for both palagonitized glass and olivine rims
585 increase steadily as a function of temperature.

586 The amount of analcime present in the tuff is positively correlated with the degree of
587 palagonitization and temperature. In contrast, phillipsite in zone 2 noticeably decreases between 1979
588 and 2017. Petrographic observations suggest, that the reason for this lies mainly in the dissolution of

589 phillipsite, with simultaneous replacement by analcime and tobermorite. This may be partially due to
590 the higher amounts of Na⁺ present in the system below sea level, which may favor the formation of
591 analcime over phillipsite. Additionally, zeolite distribution in hydrothermally altered rocks is also
592 known to be governed to a large extent by temperature (Browne, 1978; Kusakabe et al., 1981; de
593 Gennaro et al., 1999; Langella et al., 2001; Kralj, 2016). For this reason, the local dominance of
594 phillipsite over analcime in more shallow depths may also be caused by the relatively lower
595 temperatures, as phillipsite would be expected to be more stable under colder conditions, when
596 compared to analcime (Chipera and Apps, 2001). Host-rock lithology may influence the type of zeolite
597 being precipitated under low-temperature hydrothermal conditions (Browne, 1978; Reyes, 2000), such
598 as the ones present in the Surtsey hydrothermal system, but this is unlikely to contribute in any
599 significant way, as the Surtsey system is almost entirely hosted in universally poorly sorted intermediate
600 to coarse alkali basaltic lapilli-tuff, showing only minor chemical or lithological variation (Schipper et
601 al., 2015). As phillipsite appears to be an early stage alteration product, the comparatively higher
602 phillipsite contents within zone 1 may also be due to the lower degree of palagonitization and therefore
603 less advanced reaction progress.

604 In SE-01, zone 2 hosts a thin ash-rich layer of darker material that is noticeably less porous and
605 less palagonitized than the surrounding rocks at 95.4 m, which coincides with a reduction in secondary
606 mineral content (Table 1). The low porosities and therefore low permeabilities in this layer likely inhibit
607 hydrothermal circulation and locally counteract the precipitation of secondary minerals and
608 devitrification of the glass at this depth. No ash-rich layer exhibiting similar properties is observed in
609 SE-02b, implying that this feature is either transient in nature or highly localized.

610 6.1.3 Zone 3 (poorly altered zone)

611 Both cores contain a poorly altered zone that is partially unconsolidated in 1979 and lightly
612 consolidated in 2017. It encompasses the depth interval from 137.8 – 150.3 m in SE-01, but has slightly
613 shrunk in diameter in SE-02b, where it reaches between 138.4 – 150.3 m. The sideromelane of the poorly
614 altered zone remains largely unpalagonitized. Only a few thin layers of slightly palagonitized tephra are
615 observed. The lack of palagonitization and consolidation by mineral cements arguably led to the poor
616 core recovery during the 1979 drilling expedition between 140.0 – 143.8 m and 148.5 – 150.3 m (see
617 Jakobsson and Moore, 1982). In SE-02b zone 3 is slightly more consolidated, but the rocks remain
618 highly porous and friable even in 2017. In both SE-01 and SE-02b, the upper and lower boundaries of
619 zone 3 are marked by a strong enrichment in phillipsite in otherwise weakly altered tuff. In SE-02b the
620 upper phillipsite enriched interval has moved further down to 141.5 m (Table 1, Fig. 9). Phillipsite
621 contents have decreased strongly in the now more extensively altered tuff between 137 – 138 m, while
622 both tobermorite and analcime have increased in abundance. This is likely because phillipsite forms
623 mainly in the initial stages of glass alteration before becoming replaced by other phases as the reaction
624 progresses. Calcium sulphates such as anhydrite and gypsum are very common and particularly
625 characteristic for zone 3.

626 An electrical resistivity log acquired after drilling of SE-02b (Jackson et al., 2019a;
627 Weisenberger et al., 2019) indicates a change within the depth interval coinciding with zone 3.
628 According to 16s rRNA gene sequencing, roughly half of the prokaryotic community composition
629 present in rock samples from SE-02b at 148 m depth, is shared with the one in seawater around the
630 island (personal correspondence from Bergsten, 2019). However, it cannot be excluded that this is
631 caused by seawater contamination during drilling. Here it is proposed, that zone 3 most likely marks an
632 interval of high permeability and sea water recharge. This would further explain the presence of
633 anhydrite and gypsum, as Ca^{2+} and SO_4^{2-} -bearing fluids entering the system might precipitate a calcium
634 sulphate phase upon being heated due to retrograde solubility.

635 6.1.4 Zone 4 (lower palagonitization zone)

636 Zone 4, between 150.3 – 157.3 m in SE-01 and 150.3 – 177.8 m in SE-02b, shows the greatest
637 change since 1979. In SE-01 alteration behavior in zone 4 resembles that of zone 2, though overall
638 alteration is less extensive. In SE-02b both palagonitization and olivine rim formation rates are much
639 higher than predicted by the temperature-alteration-trends derived from samples in zones 1 and 2 (Fig.
640 11). The fact that this is not observed in samples from SE-01 indicates, that alteration in zone 4 has
641 increased over time. The co-appearance of all three types of palagonitized glass rims, mostly II and III,
642 arranged concentrically around sideromelane grains in the order type III → type II → type I →
643 sideromelane is common in zone 4 in SE-02b (Fig. 6). As temperature is not the driving factor for the
644 increase in alteration rates at this depth, other potential explanations may be found in chemical changes
645 in the hydrothermal fluid or potentially in the water-rock ratio of the environment (Pauly et al., 2011).

646 6.1.5 Zone 5 (bottom zone)

647 The area below zone 4 in each core contains mostly fresh and apparently unaltered
648 sideromelane. Absence of palagonitization and significant mineral cementation by zeolites and
649 tobermorite in pore space causes the tephra of this zone to be largely unconsolidated. No olivine rims
650 are detected under the microscope. Observed secondary mineralization is limited to mostly anhydrite
651 and possibly bassanite in SE-01. In SE-02b both gypsum and anhydrite are observed.

652 6.2 Olivine alteration rates

653 Olivine alteration rates were estimated by dividing olivine rim thicknesses by time (assuming a
654 12-year timespan for SE-01 and a 50-year timespan for SE-02b) and plotting the results against
655 temperature logging data from 1980 and 2018 to best approximate the current state of the system. Since
656 temperature is related to alteration rates, these values should not be taken as fully accurate representation
657 of the system's effective temperature, which varied over time. For samples from below 156.9 m, where
658 no olivine rims are found in SE-01, a time period of 38 years for the alteration is assumed instead, as
659 this value would be closer to the actual amount of time available for the alteration to progress. Our

660 results confirm a positive relationship between olivine alteration rates and temperature, as first
661 documented by Jakobsson and Moore (1986). The olivine alteration rates derived from the present study
662 are slightly higher than those given by Jakobsson and Moore (1986), which is likely due to differences
663 in methodology, specifically in the temperature values used. Regardless of the total extent of alteration
664 rates, new insights are gained regarding the nature of the olivine-clay mineral reaction in the Surtsey
665 tuff. Based on the analyses of the SE-01 core samples immediately after drilling and the temperature
666 history of the system as of 1980, Jakobsson and Moore (1986) hypothesized a threshold temperature of
667 120 ± 5 °C for the alteration of olivine to clay minerals. They cited this as a potential reason for the
668 absence of olivine rims above water level, as temperatures would not have exceeded 100 °C in that part
669 of the system. However, our data from the 2017 drill core provide evidence that olivine rim formation
670 can occur at lower temperatures within the hydrothermal system given enough time. In the SE-02b
671 samples we observe 20 – 50 µm thick alteration rims on olivine at 134.3 – 138.4 m and in zone 4 at
672 157.5 – 177.8 m. At these depths, temperatures have ranged from ca. 44 – 103 °C between 1980 and
673 2017 (Fig. 3), which is well below the threshold temperature proposed by Jakobsson and Moore (1986).
674 Temperature alone can therefore not be the reaction's sole limiting parameter.

675 Lafay et al. (2012) performed autoclave experiments on olivine under alkaline conditions at 150
676 – 200 °C to study the rate of olivine replacement during serpentinization, measuring the fraction of
677 grains <30 µm, 30 – 56 µm and 56 – 150 µm that remained after a given time interval. Their results and
678 those of Malvoisin et al. (2012) are used to estimate alteration rates for serpentinization in µm·yr⁻¹,
679 which are plotted in Figure 11 for comparison.

680 6.3 Palagonitization rates

681 Estimation of palagonitization rates was performed analogously to olivine alteration rates (see
682 above). As samples from below 156.9 m remain unpalagonitized in 1979, a timespan of 38 years,
683 between 1979 and 2017, is assumed as base for the alteration rates of these samples. It should be noted
684 that Jackson et al. (2019b) identify minimal glass alteration at this depth by using X-ray
685 microdiffraction. Palagonitization rates for samples from either drill core are correlated positively with
686 temperature and generally plot along two highly similar trendlines (Fig. 11). In their 1986 study of SE-
687 01, Jakobsson and Moore reported palagonitization rates of ca. 0.2 – 3.5 µm·yr⁻¹ for alteration rims in
688 glass lapilli. This contrasts with our results, which range between 3.33 – 42.50 µm·yr⁻¹ for samples from
689 the same drill core. It is likely that the reason for this discrepancy and that of the olivine alteration rates
690 lies in a difference in the approach used. For instance, no universal stage was employed in this study to
691 measure the exact angle of the rims. Our results nevertheless reproduce the same general trends in terms
692 of palagonitized rim thickness variations with depth. In addition, Jakobsson and Moore (1986) estimated
693 the effective temperature based on several parameters, whereas in this study a direct measurement is
694 used. These factors are thought to contribute to the deviations between the two studies.

695 Palagonitization rates of comparable magnitude to those in our study have been achieved in
696 experiments conducted by Furnes (1975) at temperatures comparable to those prevalent in Surtsey's
697 hydrothermal system. Thomassin (1984) demonstrated experimentally that a palagonitic rim "several
698 micrometers in thickness" can be formed in as little as nine months for samples heated in seawater using
699 a Teflon reactor. Malow et al. (1984) derived even higher alteration rates for samples leached in NaCl
700 solutions heated to 200 °C. Our results, though different from those of Jakobsson and Moore (1986), are
701 therefore still within established parameters.

702 6.3.1 Alteration rates in zone 4

703 Palagonitic and olivine alteration rims indicate much higher alteration rates in the tuff from
704 150.3 – 177.8 m than predicted based on temperature alone (Fig. 11). Many of these rocks remained
705 largely unaltered in 1979, meaning that the visible onset of palagonitization and olivine alteration would
706 have commenced at an unspecified time after 1979, but before 2017. From this it can be concluded that
707 the true alteration rates at this depth may be even higher than estimated here, since the alteration would
708 have occurred over a shorter time span than the assumed 38 years between 1979 and 2017. Even if
709 palagonitization and olivine rim formation have been ongoing in these areas throughout the entire 50-
710 year history of the hydrothermal system, alteration rates are still substantially higher than predicted by
711 the temperature-alteration-rate trends established by more shallow depth intervals. Possible reasons for
712 this may lie in evolving fluid compositions, such as changing salinities, or in a different water-rock ratio.

713 6.4 Palagonite maturation

714 Three different types of palagonitization are identified in the Surtsey tuff samples, which are
715 distinct in their textural and optical properties. These type I-II-III palagonitized glass rims exhibit a
716 progressively more granular to fibrous texture and less gel-like appearance. Peacock (1926) first
717 recognized two texturally distinct types of palagonite – the amorphous gel-palagonite and the slightly
718 crystalline "fibro-palagonite" – in his comprehensive review of the petrology of Icelandic tuffs. Stroncik
719 and Schmincke (2001) recognized that after the initial palagonitization process the altered glass
720 undergoes a series of aging steps over time. They state that crystallinity gradually increases as palagonite
721 ages, ultimately resulting in the complete crystallization of the material to smectite and other authigenic
722 minerals, a finding also confirmed by other workers (Singer, 1974; Berggaut et al., 1994; Crovisier et
723 al., 2003; Drief and Schiffman, 2004). The classification scheme proposed by Stroncik and Schmincke
724 (2001) uses the ratio of amorphous to crystalline material in the altered glass to delineate between the
725 initial gel-palagonite (aging step I, mostly amorphous), fibro-palagonite (aging step II, mostly
726 crystalline), and fully crystalline smectite. In their study of the palagonitic alteration of hyaloclastites
727 from Hawaii, Walton and Schiffman (2003) recognized the formation of a complex of minerals,
728 intergrown at the nanometer scale and dominantly composed of smectite, which they called 'reddened
729 smectite grain replacement' (Walton and Schiffman, 2003). This material can be considered analogous

730 to fibro-palagonite as described by Peacock (1926) (Drief and Schiffman, 2004). Despite these
731 differences in the applied classification scheme or nomenclature, these authors and many others have
732 generally agreed that the increasing crystallinity of palagonitized glass develops as the result of
733 palagonitic maturation over time by means of reaction towards equilibrium with the interfacing
734 hydrothermal fluid; only the amorphous gel-palagonite likely representing the initial alteration product
735 of sideromelane (Singer, 1974; Zhou et al., 1992; Stroncik and Schmincke, 2001; Crovisier et al., 2003;
736 Drief and Schiffman, 2004; Pauly et al., 2011).

737 Based on this large body of prior observations, we interpret the different types of palagonitic
738 textures in the Surtsey samples as indicative of progressive maturation. Type I palagonitization (or gel-
739 palagonite) marks an early stage, with type II and III representing progressively more advanced stages,
740 wherein crystallinity increases and the palagonitized glass takes on a fibrous texture, before turning an
741 earthy, mottled and opaque shade of brown as the devitrification process advances (Fig. 5). The
742 distribution of these three palagonitic types is correlated with temperature, with type I found mainly in
743 the areas of lowest temperature – especially above water level – and type III found in the areas of highest
744 temperature. An exception to this is the depth interval of rapid palagonitization in SE-02b between 150.3
745 – 177.8 m (zone 4; see above) (Fig. 10), where temperatures are low, but very little type I palagonitized
746 glass is observed. Within the framework of this interpretation, type III palagonitic rims represent a
747 highly advanced stage of the devitrification process, so that the term “palagonite” in the strict sense may
748 not be fully applicable. The very high concentration of X-ray amorphous phases in SE-01 around the
749 system’s area of maximum temperature (Grimaldi, 2018), where type III is observed, potentially
750 indicates that a large portion of the material may have recrystallized as poorly ordered clays (Brindley,
751 1977).

752 7 Summary

753 The systematic petrographic comparison of two parallel vertical drill cores from the eastern
754 tephra pile of the Surtur crater at Surtsey volcano, recovered in 1979 and 2017, provides new
755 petrographic insights into time-lapse alteration within the island’s basaltic low-temperature
756 hydrothermal system, which will serve as the basis for future geochemical analyses.

- 757 1. Five discrete zones of distinct alteration style are recognized in the two studied Surtsey drill cores.
758 These zones (Fig. 10), are defined by their discrete alteration mineralogy, development of
759 secondary phases over time, as well as alteration of basaltic glass. Their vertical positions
760 differ only slightly between the 1979 and 2017 drill cores.
- 761 2. Alteration in the form of palagonitization, zeolitization and tobermorite formation has progressed
762 rapidly in most of the zones except for parts of the poorly altered zone 3 at 138.4 – 150.3 m

763 depth, where alteration does not appear to have progressed to a significant degree from 1979
764 to 2017.

- 765 3. The rates of glass and olivine alteration, as measured by alteration rim thicknesses, generally
766 reproduce the trends established by Jakobsson and Moore (1986). Both types of alteration
767 increase with temperature in the SE-01 samples and in the SE-02b samples above zone 4 (Fig.
768 11). In zone 4 of SE-02b, alteration rates diverge from this general trend, yielding higher than
769 expected rates of production for both palagonitized glass and altered olivine rims.
- 770 4. Phillipsite appears to be an early stage alteration product, for which the relative abundance has
771 decreased in all samples between 65.4 – 138.4 m depths since 1979. This is consistent with
772 petrographic observations, which show phillipsite dissolution or alteration to analcime and
773 tobermorite.
- 774 5. Surtsey tuff samples show three principal types of palagonitized glass textures, which indicate
775 progressive stages in the reaction of sideromelane to smectite. The distribution of these three
776 palagonitic types in SE-01 and SE-02b shows clear progress in the ongoing devitrification of
777 the Surtsey tephra deposits between 1979 and 2017.

778 8 Acknowledgements

779 Funding for this project was provided by the International Continental Scientific Drilling
780 Program (ICDP) through a grant to the SUSTAIN project; a grant of excellence from the Icelandic
781 Research Fund, ICF-RANNÍS; the Bergen Research Foundation and K.G. Jebsen Centre for Deep Sea
782 Research at the University of Bergen, Norway; the German Research Foundation; and DiSTAR,
783 Federico II, University of Naples, Federico II, Italy. The University of Utah, USA, and the two Icelandic
784 power companies Reykjavík Energy and Landsvirkjun contributed additional funds. The authors would
785 like to express their gratitude to Barbara I. Kleine, Pauline Bergsten, Carolyn F. Gorny and James G.
786 Moore for constructive feedback on the topics of fluid geochemistry, microbiology and volcanology.

787

788

789 9 References

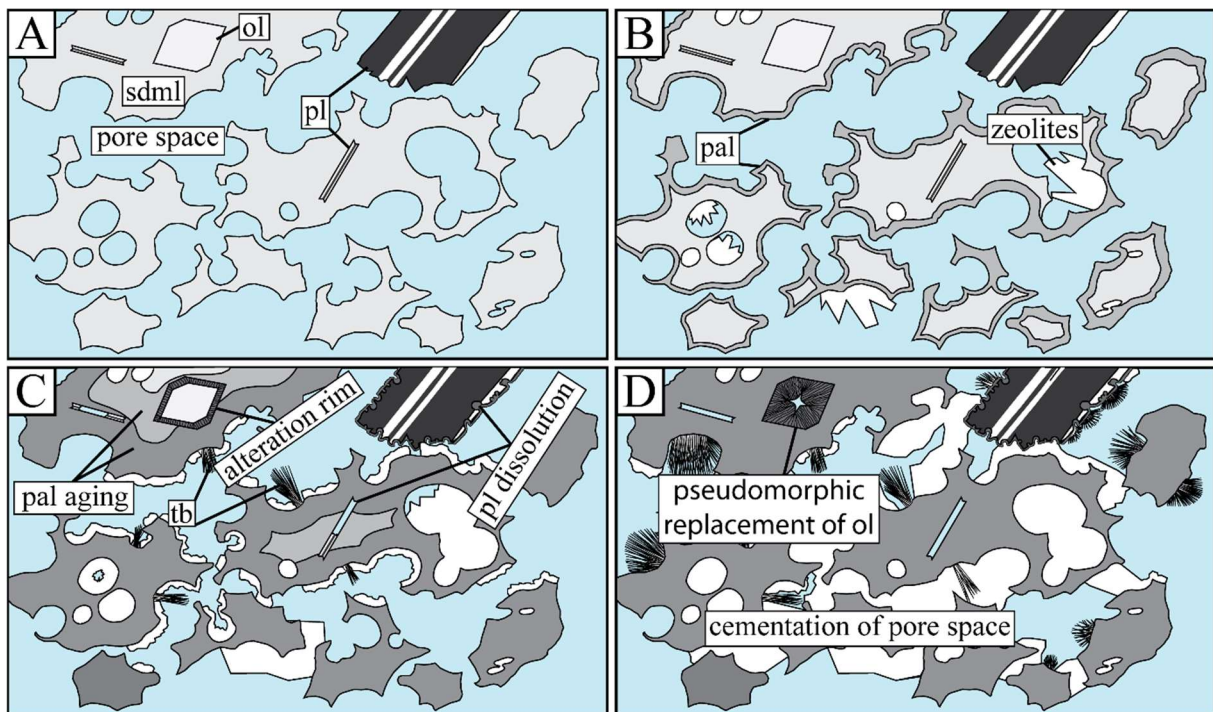
- 790 Bergsten, P., Vannier, P., Klonowski, A.M., Knobloch, S., Frion, J., Mougeolle, A., Kleine, B.I., Prause,
791 S., Stefánsson, Á., Weisenberger, T.B., Jackson, M.D., Guðmundsson, M.T., Marteinsson, V. þ.,
792 2019. Manuscript in preparation.
- 793 Berkgaunt, V., Singer, A., Stahr, K., 1994. Palagonite reconsidered: Paracrystalline illite-smectites from
794 regoliths on basic pyroclastics. *Clays Clay Miner.* 42, 582–592.
- 795 Bish, D.L., Chipera, S.J., 1987. Problems and solutions in quantitative analysis of complex mixtures by
796 X-ray powder diffraction. *Adv. X-ray Anal.* 31, 295–308.
- 797 Brindley, G.W., 1977. Aspects of order-disorder in clay minerals-a review. *Clay Science* 5, 103–112
- 798 Browne, P.R.L., 1978. Hydrothermal Alteration in Active Geothermal Fields. *Annu. Rev. Earth Planet.
799 Sci.* 6, 229–248.
- 800 Chipera, S.J., Apps, J.A., 2001. Geochemical stability of natural zeolites, in: Bish, D.L., Ming, D.W.
801 (Eds.), *Natural Zeolites: Occurrence, Properties, Applications*. pp. 117–157.
- 802 Crovisier, J.L., Eberhart, J.P., Honnorez, J., 1986. Dissolution of basaltic glass in seawater: Mechanism
803 and rate, in: *Extended Abstracts of the Fifth International Symposium on Water-Rock Interaction*.
804 International Association of Geochemistry and Cosmochemistry, Reykjavik, Iceland, pp. 142-145
- 805 Crovisier, J.L., Advocat, T., Dussossoy, J.L., 2003. Nature and role of natural alteration gels formed on
806 the surface of ancient volcanic glasses (Natural analogs of waste containment glasses). *J. Nucl.
807 Mater.* 321, 91–109.
- 808 de Gennaro, M., Langella, A., Cappelletti, P., Colella, C., 1999. Hydrothermal conversion of trachytic
809 glass to zeolite. 3. Monocationic model glasses. *Clays Clay Miner.* 47, 348–357.
- 810 Drief, A., Schiffman, P., 2004. Very low-temperature alteration of sideromelane in hyaloclastites and
811 hyalotuffs from Kilauea and Mauna Kea volcanoes: Implications for the mechanism of palagonite
812 formation. *Clays Clay Miner.* 52, 623–635.
- 813 Fisher, R. V., Schmincke, H.U., 1984. Submarine Volcaniclastic Rocks, in: *Pyroclastic Rocks*. Springer,
814 Berlin, Heidelberg, pp. 265–296.
- 815 Friedman, J.D., Williams, R.S., 1970. Changing patterns of thermal emission from Surtsey, Iceland,
816 between 1966 and 1969. *US Geol. Surv. Prof. Pap.* 700-D, 116–124.
- 817 Frolova, Y.V., 2010. Patterns of Transformations in the Compositions and Properties of Icelandic
818 Hyaloclastites during Lithogenesis. *Moscow Univ. Geol. Bull.* 65, 104–114.
- 819 Furnes, H., 1975. Experimental Palagonitization of Basaltic Glasses of Varied Composition. *Contrib. to
820 Mineral. Petrol.* 50, 105–113.
- 821 Gernon, T.M., Hincks, T.K., Tyrrell, T., Rohling, E.J., Palmer, M.R., 2016. Snowball Earth ocean
822 chemistry driven by extensive ridge volcanism during Rodinia breakup. *Nat. Geosci.* 9, 242.
- 823 Giggenbach, W.F., 1984. Mass transfer in hydrothermal alteration systems—a conceptual approach.
824 *Geochim. Cosmochim. Acta* 48, 2693–2711
- 825 Grimaldi, C., 2018. Quantitative characterizaton of zeolites from Surtsey island (Iceland). M.Sc. thesis.
826 Department of Earth, Environmental and Resources Sciences at the University of Napoli Federico
827 II, Italy.
- 828 Hekinian, R., Hoffert, M., 1975. Rate of palagonitization and manganese coating on basaltic rocks from
829 the rift valley in the Atlantic Ocean near 36°50'N. *Mar. Geol.* 19, 91–109.
- 830 Henley, R.W., Truesdell, A.H., Barton, P.B., Whitney, J.A., 1985. Fluid-Mineral Equilibria in
831 Hydrothermal Systems. *Society of Economic Geologists*.
- 832 Honnorez, J., 1978. Generation of phillipsites by palagonitization of basaltic glass in sea water and the
833 origin of K-rich deep-sea sediments, in: Sand, L.B., Mumpton, F.A. (Eds.), *Natural Zeolites:
834 Occurrence, Properties, Use*. pp. 245–258.

- 835 Jackson, M.D., Gudmundsson, M.T., Bach, W., Cappelletti, P., Coleman, N.J., Ivarsson, M., Jónasson,
836 K., Jørgensen, S.L., Marteinsson, V., McPhie, J., Moore, J.G., Nielson, D., Rhodes, J.M., Rispoli,
837 C., Schiffman, P., Stefánsson, A., Türke, A., Vanorio, T., Weisenberger, T.B., White, J.D.L.,
838 Zierenberg, R., Zimanowski, B., 2015. Time-lapse characterization of hydrothermal seawater and
839 microbial interactions with basaltic tephra at Surtsey Volcano. *Sci. Drill.* 20, 51–58.
- 840 Jackson, M.D., Guðmundsson, M.T., Weisenberger, T.B., Rhodes, J.M., Stefánsson, A., Kleine, B.I.,
841 Lippert, P.C., Marquardt, J.M., Reynolds, H.I., Kück, J., Marteinsson, V. þ., Vannier, P., Bach,
842 W., Barich, A., Bergsten, P., Bryce, J.G., Cappelletti, P., Couper, S., Fahnestock, M.F., Gorny,
843 C.F., Grimaldi, C., Groh, M., Guðmundsson, A., Gunnlaugsson, Á. þ., Hamelin, C., Högnadóttir,
844 P., Jónasson, K., Jónsson, S.S., Jørgensen, S.L., Klonowski, A.M., Marshall, B., Massey, E.,
845 McPhie, J., Moore, J.G., Ólafsson, E.S., Onstad, S.L., Perez, V., Pausse, S., Snorasson, S.P., Türke,
846 A., White, J.D.L., Zimanowski, B., 2019a. SUSTAIN drilling at Surtsey volcano, Iceland, tracks
847 hydrothermal and microbiological interactions in basalt 50 years after eruption. *Sci. Drill.* 25, 35–
848 46
- 849 Jackson, M.D., Couper, S., Stan, C.V., Ivarsson, M., Czabaj, M.W., Tamura, N., Parkinson, D., Miyagi,
850 L.M., Moore, J.G., 2019b. Authigenic mineral textures in submarine 1979 basalt drill core, Surtsey
851 volcano, Iceland: Geochemistry, Geophys., Geosystems, 20, 3751–3773
- 852 Jakobsson, S.P., 1971. Palagonitiseringen af tefraen på Surtsey. *Naturufraedistofnun Islands* 61–62.
- 853 Jakobsson, S.P., 1972. On the Consolidation and Palagonitization on the Tephra of the Surtsey Volcanic
854 Island, Iceland. *Surtsey Res. Prog. Rep.* 121–128.
- 855 Jakobsson, S.P., 1978. Environmental factors controlling the palagonitization of the Surtsey tephra,
856 Iceland. *Bull. Geol. Soc. Denmark* 27, 91–105.
- 857 Jakobsson, S.P., Moore, J.G., 1982. The Surtsey Research Drilling Project of 1979. *Surtsey Res.* 9, 76–
858 93.
- 859 Jakobsson, S.P., Moore, J.G., 1986. Hydrothermal minerals and alteration rates at Surtsey volcano,
860 Iceland. *Geol. Soc. Am. Bull.* 97, 648–659.
- 861 Jakobsson, S.P., Gudmundsson, G., Moore, J.G., 2000. Geological monitoring of Surtsey, Iceland, 1967–
862 1998. *Surtsey Res.* 11, 99–108.
- 863 Kousehlar, M., Weisenberger, T.B., Tutti, F., Mirnejad, H., 2012. Fluid control on low-temperature
864 mineral formation in volcanic rocks of Kahrizak, Iran. *Geofluids* 12, 295–311.
- 865 Kralj, P., 2016. Hydrothermal zeolitisation controlled by host-rock lithofacies in the Periadriatic
866 (Oligocene) Smrekovec submarine composite stratovolcano, Slovenia. *J. Volcanol. Geotherm.*
867 Res. 317, 53–65.
- 868 Kusakabe, H., Minato, H., Utada, M., Yamanaka, T., 1981. Phase relations of clinoptilolite, mordenite,
869 analcime and albite with increasing pH, sodium ion concentration and temperature. *Sci. Pap. Coll.*
870 *Gen. Educ. Univ. Tokyo* 31, 39–59.
- 871 Lafay, R., Montes-Hernandez, G., Janots, E., Chiriac, R., Findling, N., Toche, F., 2012. Mineral
872 replacement rate of olivine by chrysotile and brucite under high alkaline conditions. *J. Cryst.*
873 *Growth* 347, 62–72.
- 874 Langella, A., Cappelletti, P., de Gennaro, R., 2001. Zeolites in closed hydrologic systems. *Rev. Mineral.*
875 *Geochemistry* 45, 235–260.
- 876 Lorenz, V., 1974. Studies of the Surtsey tephra deposits. *Surtsey Res. Prog. Rep.* 7, 72–79.
- 877 Malow, G., Lutze, W., Ewing, R.C., 1984. Alteration effects and leach rates of basaltic glasses:
878 implications for the long-term stability of nuclear waste form borosilicate glasses. *J. Non. Cryst.*
879 *Solids* 67, 305–321.
- 880 Malvoisin, B., Brunet, F., Carlut, J., Rouméjon, S., Cannat, M., 2012. Serpentinitization of oceanic
881 peridotites: 2. Kinetics and processes of San Carlos olivine hydrothermal alteration. *J. Geophys.*
882 *Res. Solid Earth* 117.
- 883 Marshall, R.R., 1961. Devitrification of natural glass. *Geol. Soc. Am. Bull.* 72, 1493–1520.

- 884 Moore, J.G., 1966. Rate of palagonitization of submarine basalt adjacent to Hawaii. US Geol. Surv.
885 Prof. Pap. 550, D163–D171.
- 886 Moore, J.G., 1985. Structure and eruptive mechanisms at Surtsey Volcano, Iceland. Geol. Mag. 122,
887 649–661.
- 888 Moore, J.G., Fornari, D.J., Clague, D.A., (1985). Basalts from the 1877 submarine eruption of Mauna
889 Loa, Hawaii; new data on the variation of palagonitization rate with temperature. U.S. Geol. Surv.
890 Bull. 1663.
- 891 Nayudu, Y.R., 1964. Palagonite tuffs (hyaloclastites) and the products of post-eruptive processes. Bull.
892 Volcanol. 27, 391–410.
- 893 Parruzot, B., Jollivet, P., Rébiscoul, D., Gin, S., 2015. Long-term alteration of basaltic glass:
894 Mechanisms and rates. Geochim. Cosmochim. Acta 154, 28–48.
- 895 Pauly, B.D., Schiffman, P., Zierenberg, R.A., Clague, D.A., 2011. Environmental and chemical controls
896 on palagonitization. Geochemistry, Geophys. Geosystems 12.
- 897 Peacock, M.A., 1926. The petrology of Iceland, Part 1, The basic tuffs. Trans. R. Soc. Edinburgh 55,
898 53–76.
- 899 Pedersen, L.E.R., McLoughlin, N., Vullum, P.E., Thorseth, I.H., 2015. Abiotic and candidate biotic
900 micro-alteration textures in subseafloor basaltic glass: A high-resolution in-situ textural and
901 geochemical investigation. Chem. Geol. 410, 124–137.
- 902 Reyes, A.G., 2000. Petrology and mineral alteration in hydrothermal systems: From diagenesis to
903 volcanic catastrophes, United Nations University, Geothermal Training Programme.
- 904 Romagnoli, C., Jakobsson, S.P., 2015. Post-eruptive morphological evolution of island volcanoes:
905 Surtsey as a modern case study. Geomorphology 250, 384–396.
- 906 Schiffman, P., Watters, R.J., Thompson, N., Walton, A.W., 2006. Hyaloclastites and the slope stability
907 of Hawaiian volcanoes: Insights from the Hawaiian Scientific Drilling Project's 3-km drill core. J.
908 Volcanol. Geotherm. Res. 151, 217–228.
- 909 Schipper, C.I., Jakobsson, S.P., White, J.D.L., Palin, J.M., Bush-Marcinowski, T., 2015. The Surtsey
910 magma series. Sci. Rep. 5, 11498
- 911 Schipper, C.I., Le Voyer, M., Moussallam, Y., White, J.D.L., Thordarson, T., Kimura, J.I., Chang, Q.,
912 2016. Degassing and magma mixing during the eruption of Surtsey Volcano (Iceland, 1963–1967):
913 the signatures of a dynamic and discrete rift propagation event. Bull. Volcanol. 78, 2–15.
- 914 Singer, A., 1974. Mineralogy of palagonitic material from the Golan Heights, Israel. Clays Clay Miner.
915 22, 231–240.
- 916 Singer, A., Banin, A., 1990. Characteristics and mode of palagonite - A review. Sci. Géologiques, Bull.
917 mémoires 88, 173–181.
- 918 Spürgin, S., Weisenberger, T.B., Marković, M., 2019. Zeolite-group minerals in phonolite-hosted
919 deposits of the Kaiserstuhl Volcanic Complex, Germany. Am. Mineral. 104, 659–670.
- 920 Staudigel, H., Hart, S.R., 1983. Alteration of basaltic glass: Mechanisms and significance for the oceanic
921 crust-seawater budget. Geochim. Cosmochim. Acta 47, 337–350.
- 922 Staudigel, H., Furnes, H., McLoughlin, N., Banerjee, N.R., Connell, L.B., Templeton, A., 2008. 3.5
923 billion years of glass bioalteration: Volcanic rocks as a basis for microbial life? Earth-Science Rev.
924 89, 156–176.
- 925 Stefánsson, V., Axelsson, G., Sigurdsson, O., Guðmundsson, G., Steingrímsson, B., 1985. Thermal
926 condition of Surtsey. Journal of Geodynamics .4, 91-106.
- 927 Stroncik, N.A., Schmincke, H.U., 2001. Evolution of palagonite: Crystallization, chemical changes, and
928 element budget. Geochemistry, Geophys. Geosystems 2.
- 929 Stroncik, N.A., Schmincke, H.U., 2002. Palagonite - a review. Int. J. Earth Sci. 91, 680–697.
- 930 Techer, I., Lancelot, J., Clauer, N., Liotard, J.M., Advocat, T., 2001. Alteration of a basaltic glass in an
931 argillaceous medium: The Salagou dike of the Lodève Permian Basin (France). Analogy with an

- 932 underground nuclear waste repository. *Geochim. Cosmochim. Acta* 65, 1071–1086.
- 933 Thomassin, J.H., 1984. Étude expérimentale de l'altération des verres silicatés dans l'eau douce et en
934 milieu océanique: apports des méthodes d'analyse de surface des solides, Thèse Doc. ès Sci.
- 935 Thorarinsson, S., 1965. Some facts about the Surtsey eruption. *Naturufraedingurinn* 35, 153.
- 936 Thorarinsson, S., Einarsson, T., Sigvaldason, G., Elisson, G., 1964. The submarine eruption off the
937 Vestmann Islands 1963-64. *Bull. Volcanol.* 27, 435–445.
- 938 Thorseth, I.H., Furnes, H., Tumyr, O., 1991. A textural and chemical study of Icelandic palagonite of
939 varied composition and its bearing on the mechanism of the glass-palagonite transformation.
940 *Geochim. Cosmochim. Acta* 55, 731–749.
- 941 Thorseth, I.H., Furnes, H., Heldal, M., 1992. The importance of microbiological activity in the alteration
942 of natural basaltic glass. *Geochim. Cosmochim. Acta* 56, 845–850.
- 943 Türke, A., Nakamura, K., Bach, W., 2015. Palagonitization of Basalt Glass in the Flanks of Mid-Ocean
944 Ridges: Implications for the Bioenergetics of Oceanic Intracrustal Ecosystems. *Astrobiology* 15,
945 793–803.
- 946 Von Waltershausen, S., 1845. Ueber die submarinen vulkanischen Ausbrüche in der Tertiär-Formation
947 des Val di Noto im Vergleich mit verwandten Erscheinungen am Aetna. *Göttinger Studien*.
- 948 Walton, A.W., Schiffman, P., 2003. Alteration of hyaloclastites in the HSDP 2 Phase 1 Drill Core 1.
949 Description and paragenesis. *Geochemistry, Geophys. Geosystems* 4.
- 950 Walton, A.W., Schiffman, P., Macpherson, G.L., 2005. Alteration of hyaloclastites in the HSDP 2 Phase
951 1 Drill Core: 2. Mass balance of the conversion of sideromelane to palagonite and chabazite.
952 *Geochemistry, Geophys. Geosystems* 6.
- 953 Weisenberger, T.B., Selbakk, R.S., 2009. Multi-stage zeolite facies mineralization in the Hvalfjördur
954 area, Iceland. *Int. J. Earth Sci.* 98, 985–999.
- 955 Weisenberger, T.B., Guðmundsson, M.T., Jackson, M.D., Gorny, C.F., Türke, A., Kleine, B.I.,
956 Marshall, B., Jørgensen, S.L., Marteinsson, V. þ., Stefánsson, A., White, J.D.L., Barich, A.,
957 Bergsten, P., Bryce, J., Couper, S., Fahnestock, M.F., Franzson, H., Grimaldi, C., Groh, M.,
958 Guðmundsson, Á., Gunnlaugsson, Á. þ., Hamelin, C., Högnadóttir, Þ., Jónasson, K., Jónsson, S.S.,
959 Klonowski, A.M., Kück, J., Magnússon, R.L., Massey, E., McPhie, J., Ólafsson, E.S., Onstad,
960 S.L., Prause, S., Perez, V., Rhodes, J.M., Snorrason, S.P., 2019. Operational Report for the 2017
961 Surtsey Underwater volcanic System for Thermophiles, Alteration processes and INnovative
962 Concretes (SUSTAIN) drilling project at Surtsey Volcano, ICDP Operational Report. DOI:
963 <http://doi.org/10.2312/ICDP.5059.001>
- 964 Whitney, D.L., Evans, B.W., 2010. Abbreviations for names of rock-forming minerals. *Am. Mineral.*
965 95, 185–187.
- 966 Zhou, Z., Fyfe, W.S., Tazaki, K., Van der Gaast, S.J., 1992. The structural characteristics of palagonite
967 from DSDP Site 335. *Can. Mineral.* 30, 75–81.
- 968
- 969
- 970

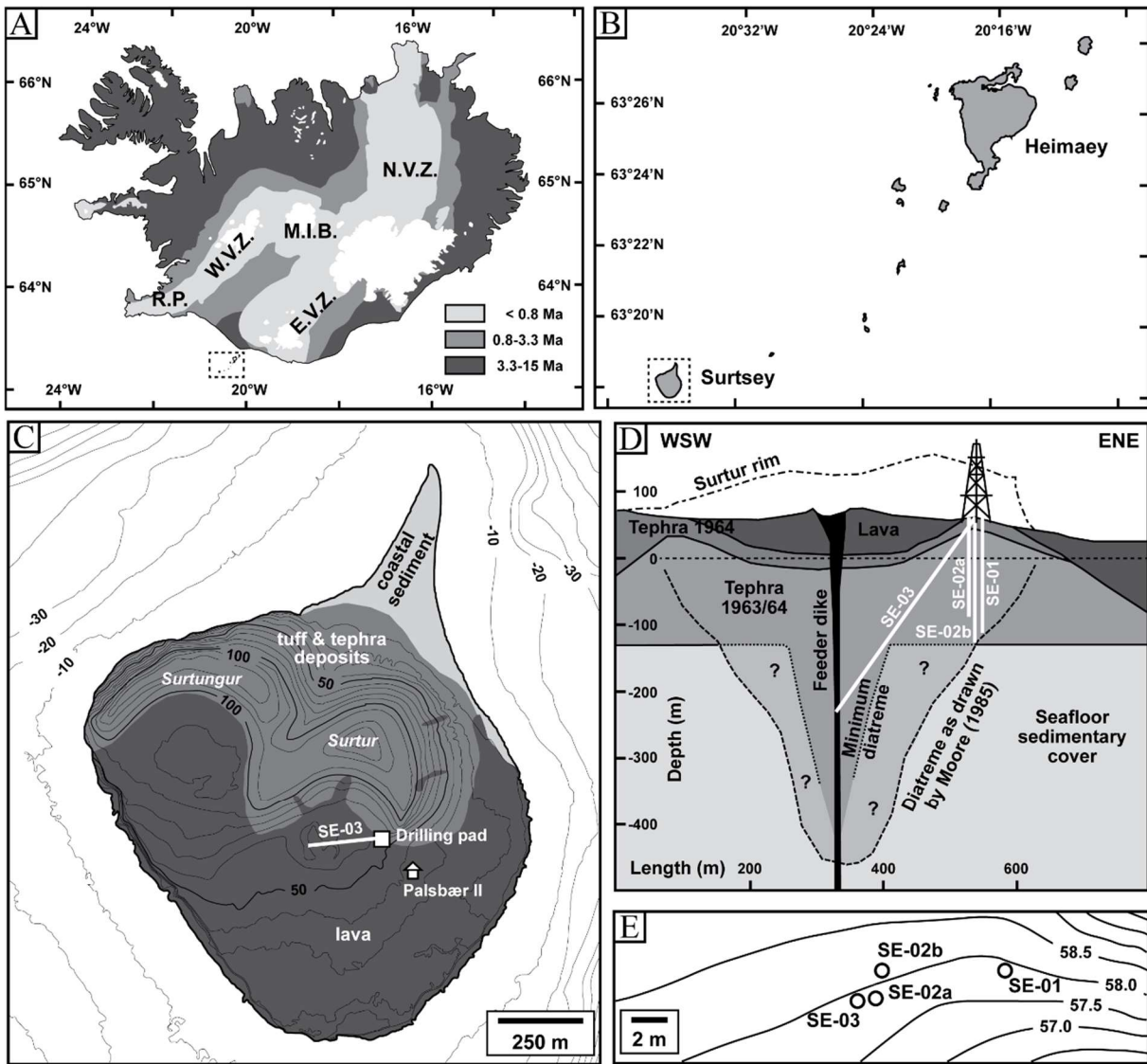
971 10 Figure captions



972

973 **Figure 1.** Schematic outline of progressive alteration of vitric tephra deposits at Surtsey: A) Fresh,
 974 unaltered tephra, composed of sideromelane (sdml) and containing (micro-)phenocrysts of primary
 975 minerals, principally olivine (ol) and plagioclase (pl). B) Incipient stage of palagonitization, marked by
 976 the presence of thin amorphous gel-palagonite rims and scattered zeolite surface coatings. C)
 977 Progression of palagonitization with ongoing glass alteration and maturation of gel-palagonite rims.
 978 Zeolite cements become increasingly widespread and tobermorite (tb) begins to crystallize. Plagioclase
 979 dissolves, forming a thin coating of phyllosilicate minerals on the crystal surface of larger crystals,
 980 while smaller crystals dissolve and leave voids within palagonitized glass. Below water level clay
 981 minerals form rims around olivine crystals and progressively encroach over time. D) More advanced
 982 alteration, most sideromelane has undergone palagonitization and most olivine grains have been altered
 983 to clay minerals. Cementation of the pore space is extensive, leading to a high degree of consolidation
 984 of the tuff and fortifying the material against erosion. The width of each images corresponds to about 5
 985 mm. Mineral Abbreviations, where applicable, after Whitney and Evans (2010).

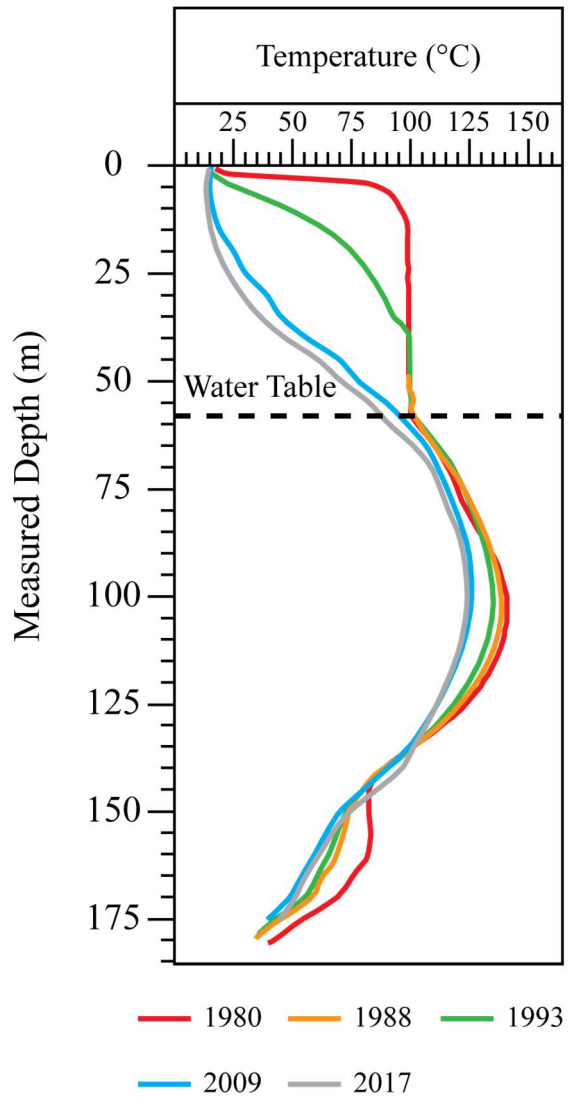
986



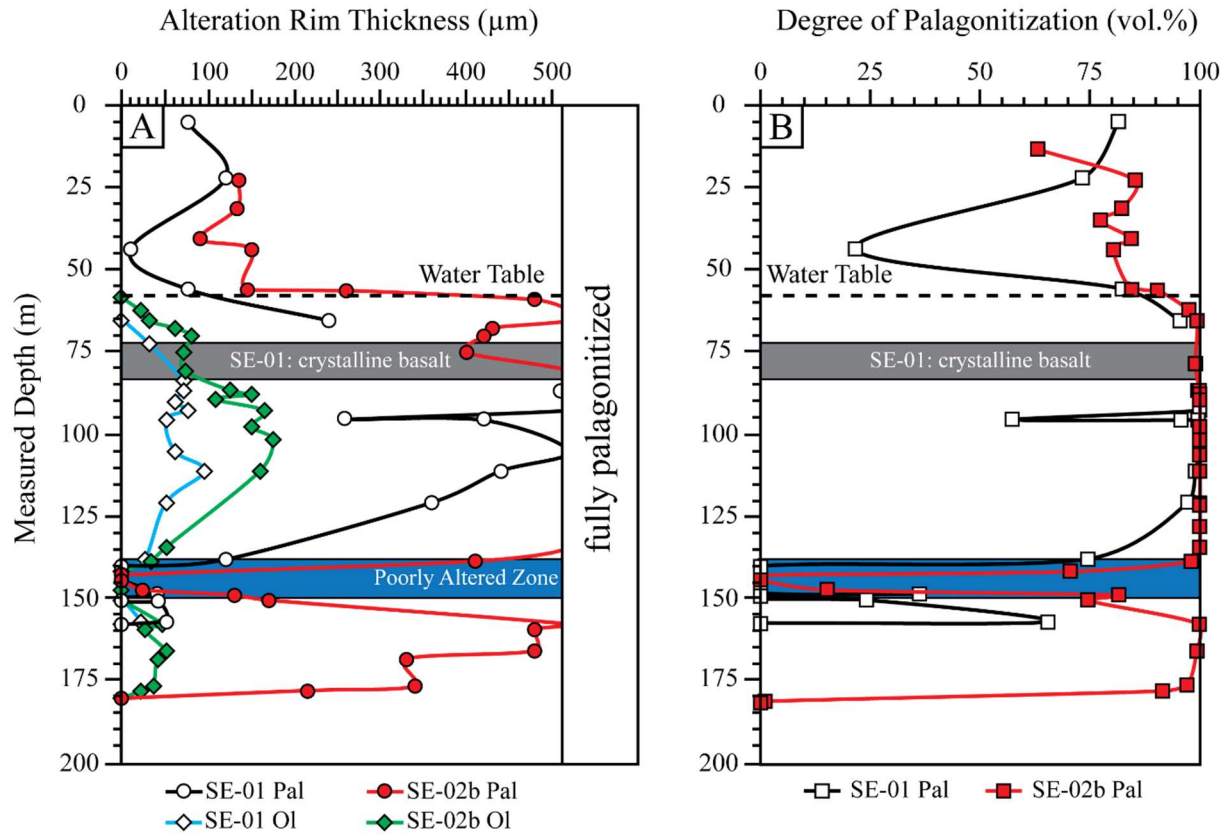
987

988 **Figure 2.** Overview of Surtsey and the 1979 and 2017 drilling projects. A) Simplified geological map
 989 showing the age distribution of rocks in greater Iceland in Ma and the main volcanic provinces (N.V.Z.:
 990 North Volcanic Zone, M.I.B.: Mid-Iceland Belt, W.V.Z.: West Volcanic Zone, E.V.Z.: East Volcanic
 991 Zone, R.P.: Reykjanes Peninsula). The Vestmannaeyjar archipelago (dashed rectangle) marks the
 992 southern seaward extension of the E.V.Z. B) The Surtsey eruptions form the southernmost extension of
 993 the archipelago. C) Geologic map of Surtsey highlighting the position of the drill pad and the Pálsbær
 994 II hut. D) Schematic cross-section through the Surtur tephra cone showing depth and orientation of the
 995 boreholes as well as the island's subsurface structure, based on Moore (1985). The drill holes from
 996 1979 (SE-01) and 2017 (SE-02a, SE-02b and SE-03) are situated in close proximity at the eastern edge
 997 of the Surtur tephra pile. E) The relative position of the boreholes. After Jackson et al. (2019a) and
 998 Weisenberger et al (2019).

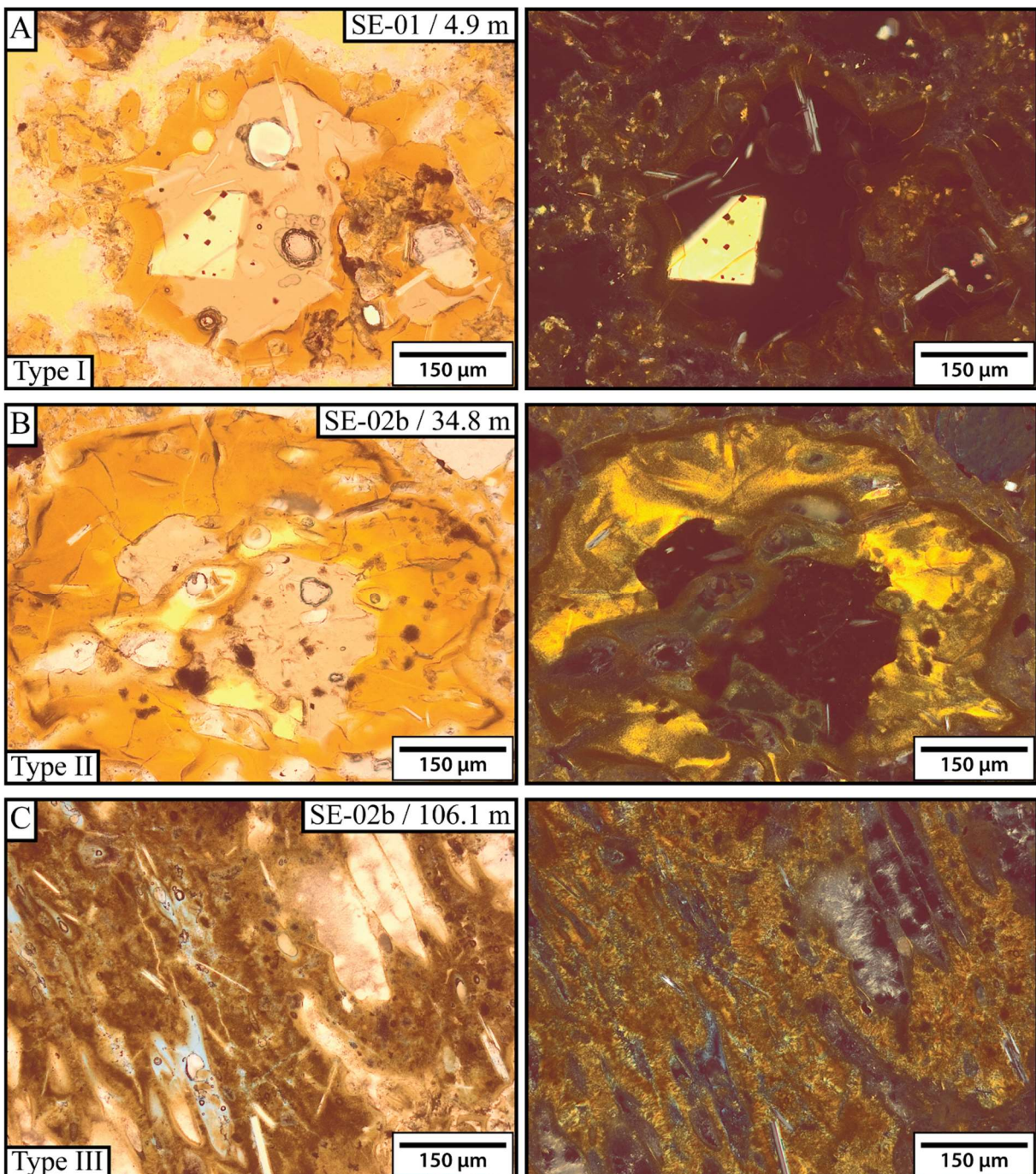
999



1000
1001 **Figure 3.** Borehole temperature profiles for SE-01 obtained between 1980 and 2017 by downhole
1002 logging.
1003



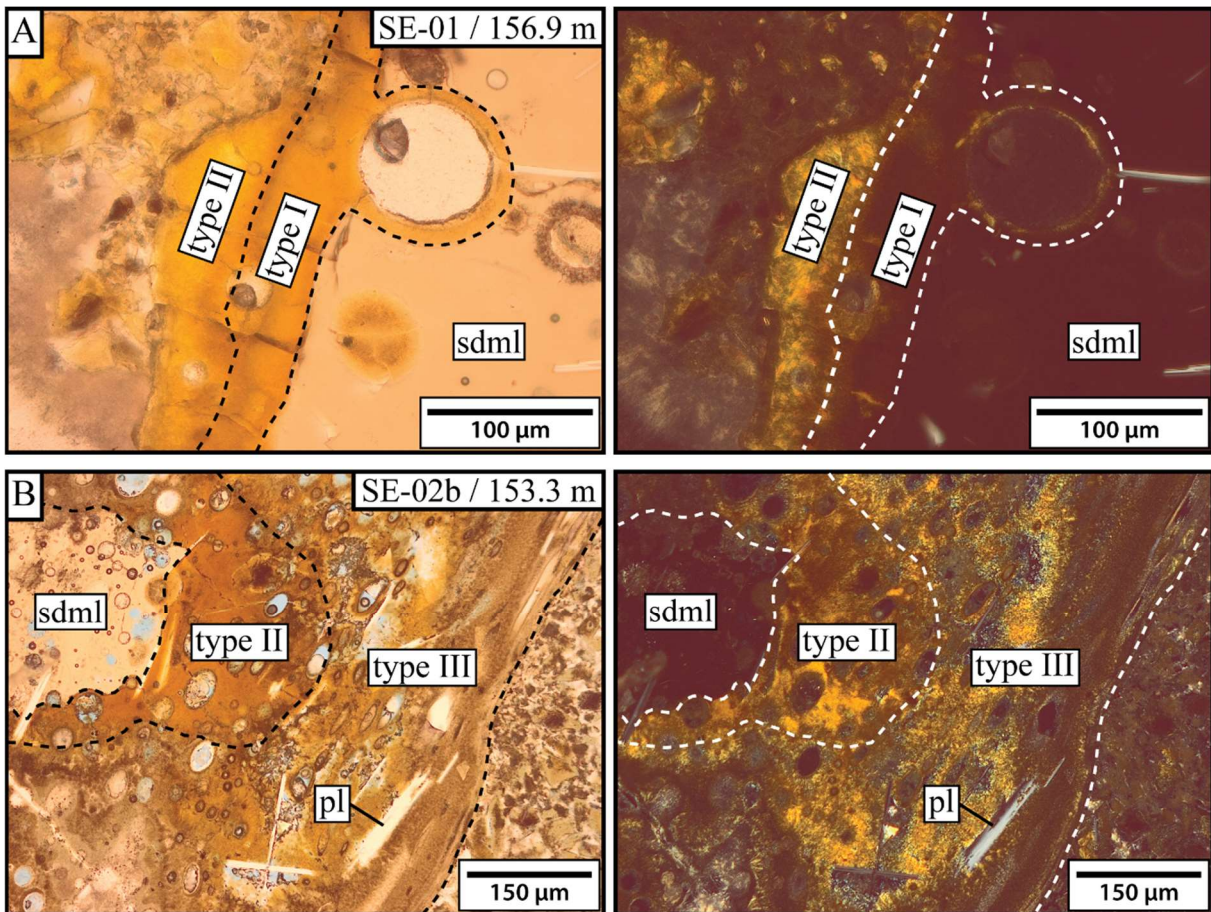
1006 **Figure 4.** A) Thicknesses of palagonitization rims on altered glass lapilli and clay mineral rims on
1007 olivine crystals in the archived 1979 SE-01 drill core and the 2017 drill core, SE-02b, plotted versus
1008 depth and measured through petrographic studies of thin sections. In both drill cores, several samples
1009 from the poorly altered zone contain neither palagonitic nor olivine rims. B) Comparison of the
1010 measured degree of palagonitization with depth between SE-01 and SE-02b.
1011



1012

1013 **Figure 5.** Three different types of palagonitized glass recognized in the Surtsey samples. A) Type I, or
 1014 gel-palagonite, is mainly isotropic and shows little to no birefringence. B) Type II, showing bright and
 1015 high intensity interference colors reminiscent of clay minerals as well as a weakly granular to fibrous
 1016 texture. C) Type III, displaying less intense interference colors, pronounced fibrous texture and a
 1017 slightly opaque, mottled appearance.

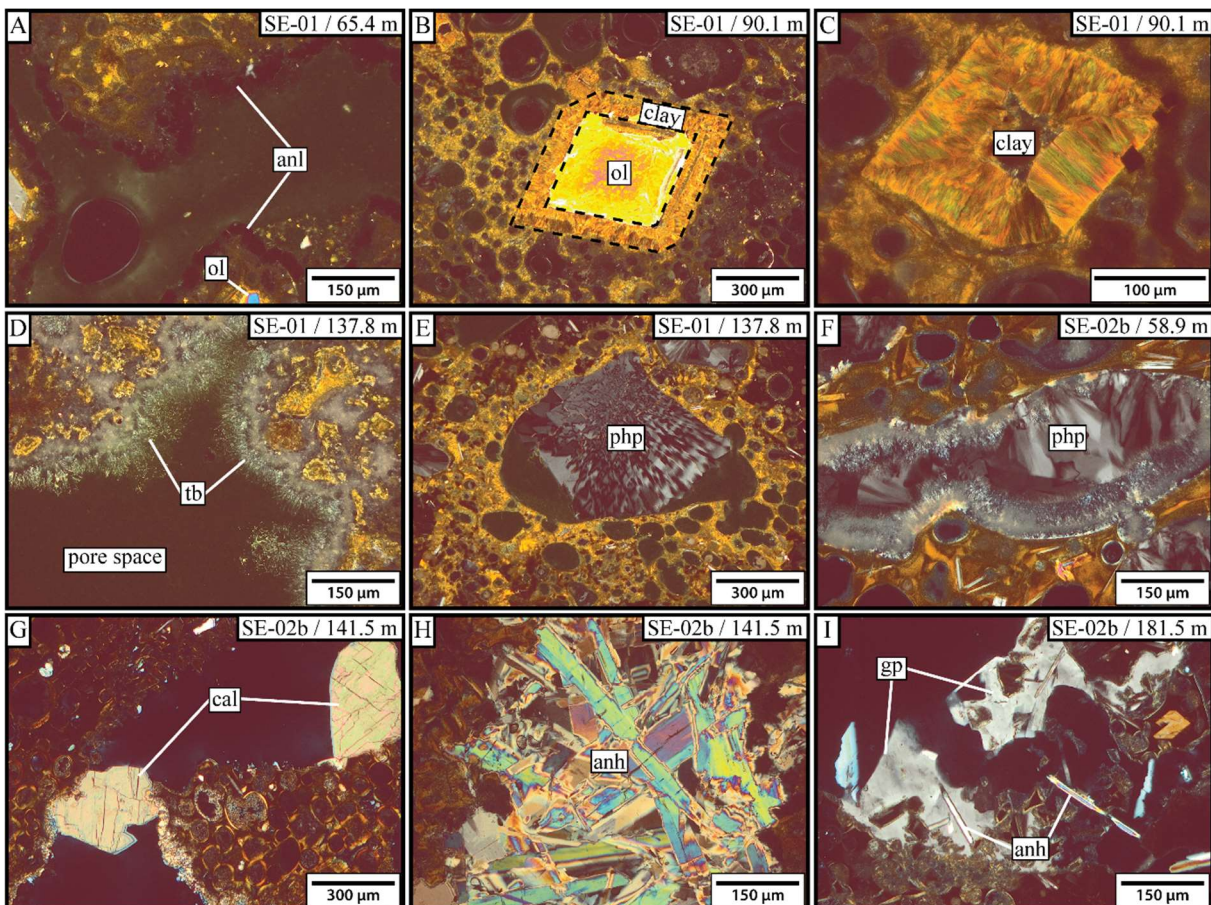
1018



1019

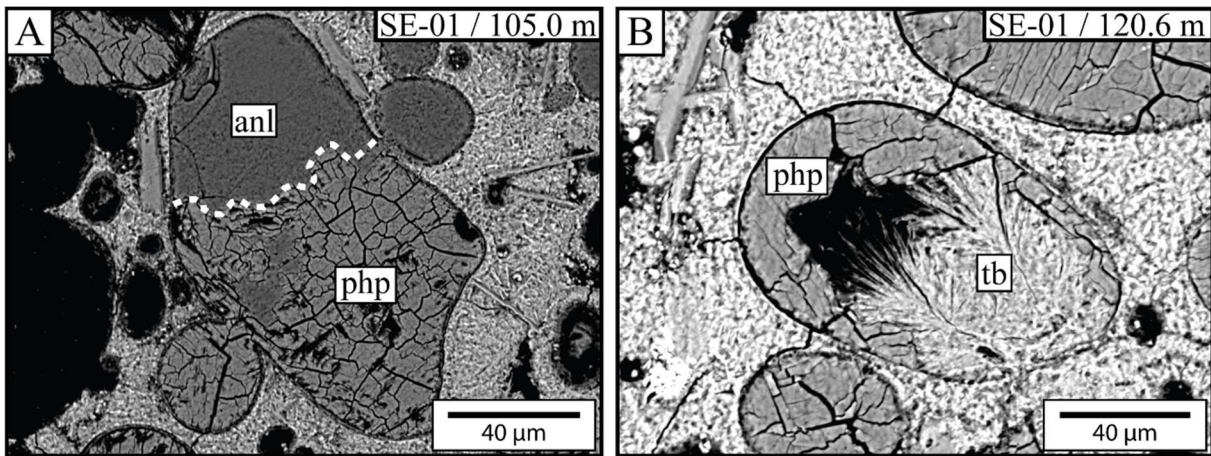
1020 **Figure 6.** Spatial relationships between the three different types of palagonitized glass textures. Where
 1021 these occur together in the same lapillus, types I-III are typically concentrically arranged around
 1022 sideromelane (i.e. seemingly “fresh” glass) in the sequence “type III → type II → type I →
 1023 sideromelane” starting at the outer edge of the grain and moving towards the glass-palagonite interface.
 1024 This observation is consistent with a model of progressive palagonite maturation, in which gel-
 1025 palagonite, i.e. type I, is first formed along the glass-fluid interface, before undergoing a continuum of
 1026 alteration processes over time and forming types II-III as the palagonitization front progresses inwards
 1027 towards the core of fresh glass in the basaltic lapillus.

1028



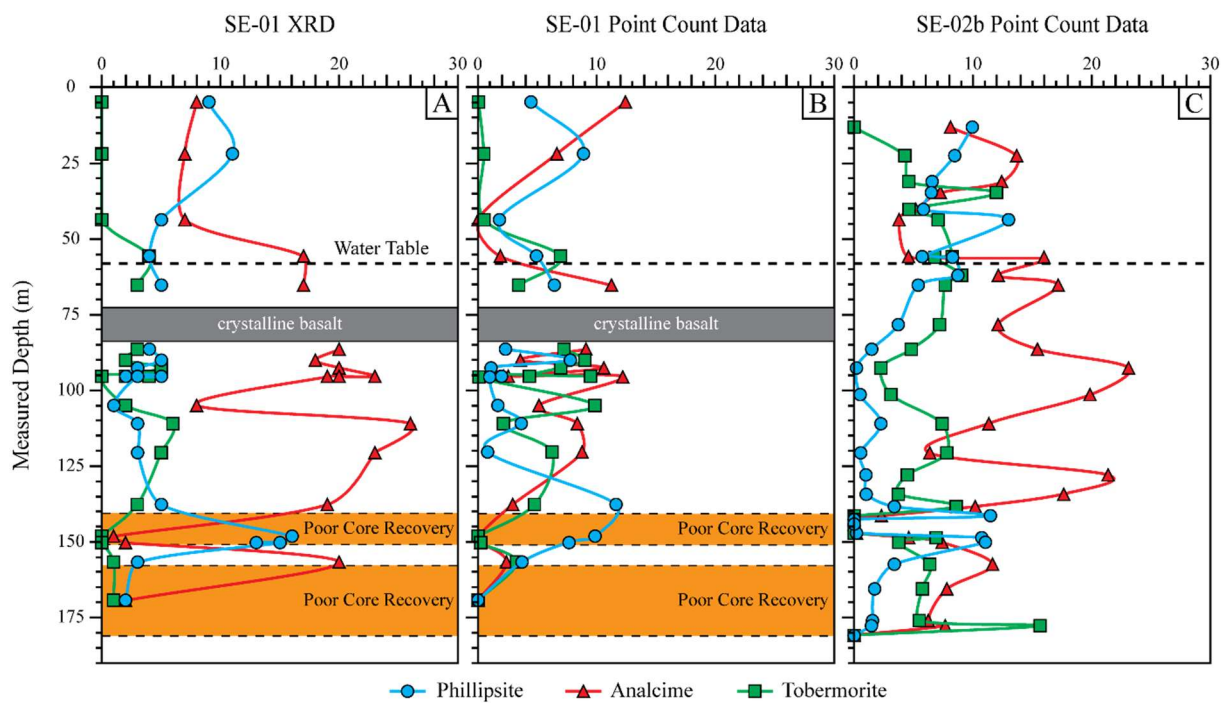
1029

1030 **Figure 7.** Overview of the most common authigenic minerals in Surtsey tuff from the archived 1979 SE-
 1031 01 drill core and the 2017 SE-02b drill core. A) Optically isotropic analcime surface textures in pores.
 1032 B) Clay mineral alteration rim on an olivine single crystal. C) Nearly complete pseudomorphic
 1033 alteration of olivine to clay minerals. D) Acicular tobermorite surface texture in a pore. E) Prismatic
 1034 phillipsite in a vesicle. F) Precipitation of phillipsite in a pore with tobermorite surface texture and
 1035 subsequent dissolution below water level. G) Massive calcite in the poorly altered zone. F) Prismatic
 1036 intergrowths of anhydrite from the poorly altered zone. G) Gypsum and anhydrite near the base of the
 1037 SE-02b drill hole. Mineral Abbreviations, where applicable, after Whitney and Evans (2010)
 1038



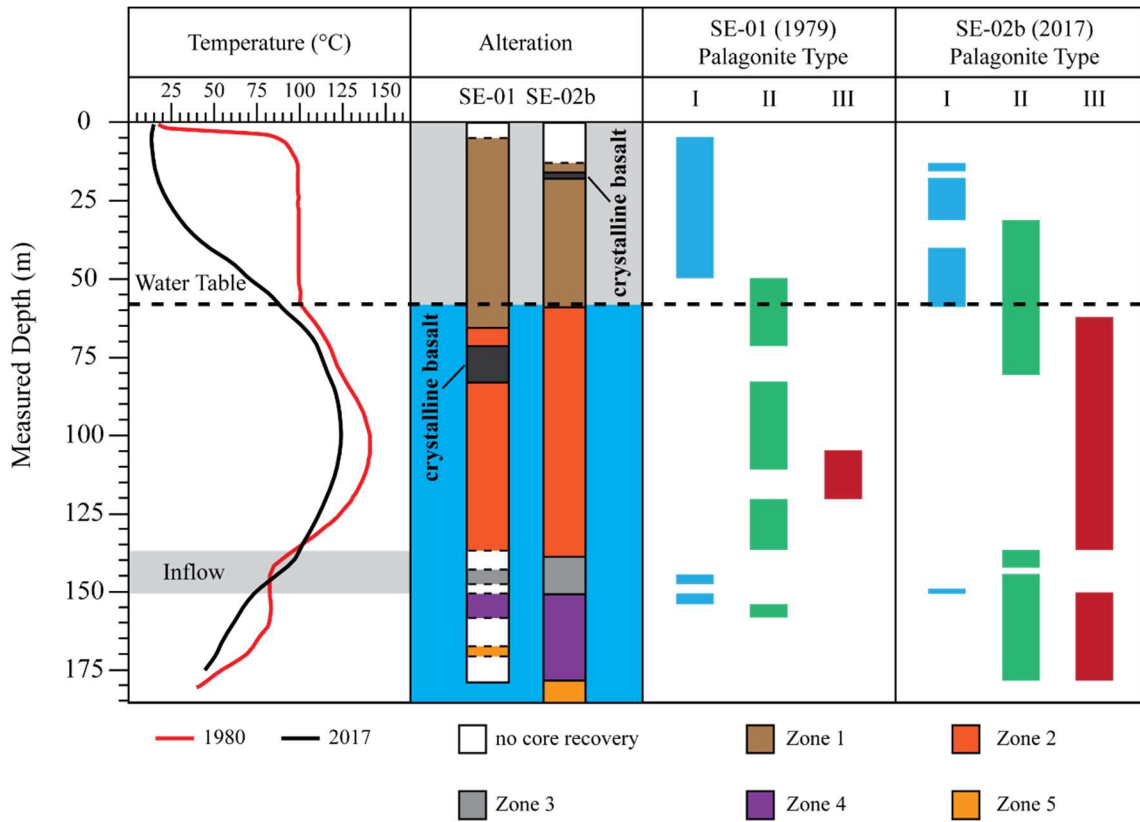
1039

1040 **Figure 8.** Backscatter electron micrograph showing A) the partial alteration of phillipsite to analcime
1041 in a lapillus vesicle and B) the growth of tobermorite in a vesicle with phillipsite surface texture.



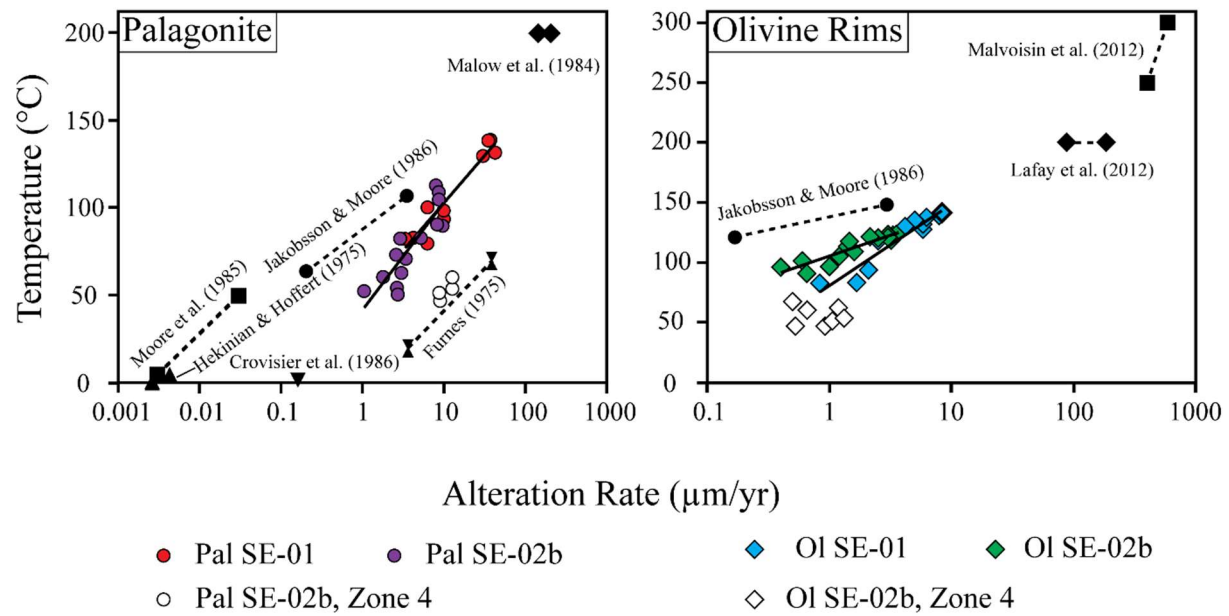
1042

1043 **Figure 9.** Relative distributions of phillipsite, analcime and tobermorite in the Surtsey drill cores based
1044 on A) x-ray diffraction (wt.%) and B) & C) point counts (vol.%). The point count data is provided as
1045 pore space free. Overall, analcime content has increased at nearly all depths. Phillipsite content has
1046 increased only in certain samples above 65.4 m depth. SE-02b contains slightly less phillipsite than SE-
1047 in the depth interval between 65.4 and 138.4 m. The top and bottom of the poorly altered zones
1048 situated between about 138-150 m show increases in phillipsite, but no increase in analcime and
1049 tobermorite. Tobermorite has mostly increased above water level and towards the bottom of the drill
1050 hole, but has decreased overall in the area of maximum temperature. Due to incomplete core recovery
1051 in SE-01 only cutting samples were available at some depth intervals within the poorly altered zone and
1052 towards the bottom of the drill core. For more information on the exact depths, refer to Table 1.



1053

1054 **Figure 10.** Integrated log displaying the relationship between temperature, alteration progress and
 1055 maturation of palagonitized glass determined through petrographic investigations of thin sections in the
 1056 archived 1979 SE-01 drill core and the 2017 SE-02b drill core.
 1057



1060 **Figure 11.** Alteration rates inferred from the thicknesses of authigenic rims on palagonitized glass
 1061 lapilli and olivine as a function of temperature for samples from the archived 1979 SE-01 and the SE-
 1062 02b drill cores and comparison with results from other studies. While a trend for the alteration rates as
 1063 a function of temperature can be reconciled for most depths, the samples retrieved from zone 4 show
 1064 higher alteration rates than what would be predicted based on the trends established by samples from
 1065 more shallow depths.

11 Tables

Table 1 Samples and petrographic results from optical thin section microscopy.

Drill hole	Depth (m)	IGSN #	Rock type	Sample type	Primary minerals (vol.%)	Glass Alteration (vol.%)		Secondary minerals (vol.%)					Porosity (vol.%)	Degree of palagonitization (vol.%)	Palagonitization extent** (vol.%)	Rim thickness (µm)	
						(Pl+Cpx+Ol)*	Sdml*	Pal*	Php*	Anl*	Tb*	Anh*	Gp*			Pal*	Ol*
SE-01	4.9	-	Lapilli-Tuff	Core	4.5	9.7	42.9	3.1	8.6	0.0	0.2	n.a.	31.1	81.5	84.9	75.0	0.0
SE-01	22.0	-	Lapilli-Tuff	Core	3.2	12.8	35.1	5.5	4.1	0.3	1.4	n.a.	37.6	73.3	77.9	120.0	0.0
SE-01	43.6	-	Lapilli-Tuff	Core	2.4	48.5	13.4	1.2	0.0	0.3	0.3	n.a.	33.9	21.6	23.5	8.8	0.0
SE-01	55.8	-	Lapilli-Tuff	Core	4.6	10.0	46.8	3.5	1.4	5.0	0.3	n.a.	28.4	82.4	85.0	75.0	0.0
SE-01	65.4	-	Lapilli-Tuff	Core	4.7	2.2	47.7	4.5	7.8	2.4	0.4	n.a.	30.2	95.5	96.5	240.0	0.0
SE-01	72.4	-	Lapilli-Tuff	Core	5.6	0.0	57.6	10.2	0.0	0.0	0.5	n.a.	26.2	100.0	100.0	n.a.	30.0
SE-01	72.4	-	Crystalline basalt	Core	95.1	0.0	0.0	0.0	0.0	1.9	1.0	n.a.	2.0	n.a.	n.a.	n.a.	n.a.
SE-01	76.1	-	Crystalline basalt	Core	96.4	0.0	0.0	0.0	0.0	0.1	0.0	n.a.	3.6	n.a.	n.a.	n.a.	n.a.
SE-01	83.5	-	Crystalline basalt	Core	96.1	0.0	0.0	0.0	0.0	0.4	1.3	n.a.	2.1	n.a.	n.a.	n.a.	n.a.
SE-01	83.5	-	Lapilli-Tuff	Core	3.7	0.0	57.9	1.2	10.4	0.0	5.3	n.a.	21.5	100.0	100.0	n.a.	70.0
SE-01	86.6	-	Lapilli-Tuff	Core	3.8	0.3	53.4	1.7	6.7	5.3	2.2	n.a.	26.6	99.5	99.6	510.0	70.0
SE-01	90.1	-	Lapilli-Tuff	Core	1.4	0.0	56.7	5.7	2.6	6.7	0.9	n.a.	26.0	100.0	100.0	n.a.	60.0

SE-01	92.6	-	Lapilli-Tuff	Core	3.1	0.0	55.7	0.8	7.8	5.2	1.4	n.a.	26.0	100.0	100.0	n.a.	75.0
SE-01	95.4	-	Lapilli-Tuff	Core	15.3	26.4	35.4	1.7	1.8	3.7	0.0	n.a.	15.8	57.3	61.7	n.a.	50.0
SE-01	95.5	-	Lapilli-Tuff	Core	3.7	2.9	64.4	1.6	2.1	7.8	0.0	n.a.	17.5	95.7	96.4	257.5	n.a.
SE-01	95.6	-	Lapilli-Tuff	Core	3.3	0.2	52.3	0.8	9.7	0.1	12.8	n.a.	20.9	99.6	99.7	420.0	n.a.
SE-01	105.0	-	Lapilli-Tuff	Core	3.8	0.0	52.3	1.2	3.7	7.1	4.3	n.a.	27.6	100.0	100.0	n.a.	60.0
SE-01	111.0	-	Lapilli-Tuff	Core	0.9	0.6	61.5	2.7	6.1	1.6	0.1	n.a.	26.6	99.0	99.2	440.0	95.0
SE-01	120.6	-	Lapilli-Tuff	Core	3.6	1.5	56.1	0.6	6.4	4.5	0.1	n.a.	27.2	97.3	97.8	360.0	50.0
SE-01	137.8	-	Lapilli-Tuff	Core	11.2	14.0	41.0	9.6	2.4	3.9	0.2	n.a.	17.7	74.6	80.3	120.0	25.0
SE-01	140.0 - 141.0	-	Lapilli-Tuff	Cuttings	n.a.	n.a.	0.0	0.0									
SE-01	143.0 - 144.0	-	Lapilli-Tuff	Cuttings	n.a.	n.a.	0.0	0.0									
SE-01	148.0 - 149.0	-	Lapilli-Tuff	Cuttings	n.a.	n.a.	0.0	0.0									
SE-01	148.3	-	Lapilli-Tuff	Core	5.4	43.3	24.6	8.1	0.0	0.0	0.7	n.a.	17.9	36.2	43.0	40.0	0.0
SE-01	149.0 - 150.0	-	Lapilli-Tuff	Cuttings	n.a.	n.a.	0.0	0.0									
SE-01	150.3	-	Lapilli-Tuff	Core	5.4	47.8	15.2	5.9	0.2	0.0	2.5	n.a.	23.1	24.1	30.8	40.0	0.0
SE-01	156.9	-	Lapilli-Tuff	Core	7.4	23.2	43.8	3.0	2.0	2.7	0.0	n.a.	18.0	65.4	69.0	50.0	20.0
SE-01	157.3 - 158.0	-	Lapilli-Tuff	Cuttings	n.a.	n.a.	0.0	0.0									
SE-01	165.0 - 166.0	-	Lapilli-Tuff	Cuttings	n.a.	n.a.	0.0	0.0									
SE-01	169.5	-	Lapilli-Tuff	Core	4.0	55.7	0.0	0.0	0.0	0.0	19.6	n.a.	20.6	0.0	0.0	0.0	0.0
SE-01	176.5-177.7	-	Lapilli-Tuff	Cuttings	n.a.	n.a.	0.0	0.0									
SE-01	178.7-180.1	-	Lapilli-Tuf	Cuttings	n.a.	n.a.	0.0	0.0									

SE-02b	13.2	ICDP5059EX3J001	Lapilli-Tuff	Core	5.6	18.3	31.4	6.8	5.6	0.0	0.9	0.0	31.4	63.1	70.5	52.5	0.0
SE-02b	22.6	ICDP5059EX1A701	Lapilli-Tuff	Core	6.9	7.5	43.6	6.8	10.9	3.4	0.9	0.0	20.0	85.3	89.6	135.0	0.0
SE-02b	31.2	ICDP5059EX7J001	Lapilli-Tuff	Core	5.8	9.5	44.1	5.2	9.8	3.6	0.1	1.1	20.7	82.2	86.8	132.5	0.0
SE-02b	34.8	ICDP5059EXBA701	Lapilli-Tuff	Core	5.2	11.5	39.3	5.0	5.6	9.3	1.4	0.0	22.6	77.4	83.8	n.a.	0.0
SE-02b	40.4	ICDP5059EX8J001	Lapilli-Tuff	Core	6.6	9.7	52.7	4.8	4.3	3.8	0.2	0.2	17.7	84.4	87.1	90.0	0.0
SE-02b	43.7	ICDP5059EXLA701	Lapilli-Tuff	Core	6.8	9.4	38.6	9.4	2.7	5.1	0.3	0.0	27.7	80.4	85.6	150.0	0.0
SE-02b	56.0	ICDP5059EXVA701	Lapilli-Tuff	Core	3.9	8.5	46.2	4.1	3.3	6.0	0.4	0.0	27.7	84.5	87.6	145.0	0.0
SE-02b	56.1	ICDP5059EXGJ001	Lapilli-Tuff	Core	5.2	4.7	44.7	6.5	12.6	5.4	0.0	0.0	20.8	90.4	93.6	260.0	0.0
SE-02b	58.9	ICDP5059EXHJ001	Lapilli-Tuff	Core	n.a.	n.a.	480.0	0.0									
SE-02b	62.1	ICDP5059EXIJ001	Lapilli-Tuff	Core	5.1	1.2	49.1	6.9	9.6	7.2	0.0	0.0	20.9	97.6	98.3	n.a.	20.0
SE-02b	65.4	ICDP5059EX5B701	Lapilli-Tuff	Core	4.3	0.3	52.7	4.4	14.1	6.3	0.0	0.0	17.9	99.4	99.6	n.a.	30.0
SE-02b	67.5	ICDP5059EXJJ001	Lapilli-Tuff	Core	n.a.	n.a.	430.0	60.0									
SE-02b	70.1	ICDP5059EXLJ001	Lapilli-Tuff	Core	n.a.	n.a.	420.0	80.0									
SE-02b	75.0	ICDP5059EXMJ001	Lapilli-Tuff	Core	n.a.	n.a.	400.0	70.0									
SE-02b	78.4	ICDP5059EXFB701	Lapilli-Tuff	Core	9.2	0.5	51.3	2.9	9.6	5.7	0.1	0.0	20.6	99.1	99.3	n.a.	n.a.
SE-02b	80.5	ICDP5059EXNJ001	Lapilli-Tuff	Core	n.a.	n.a.	n.a.	72.5									
SE-02b	86.5	ICDP5059EXPB701	Lapilli-Tuff	Core	2.3	0.0	61.4	1.2	12.6	3.9	0.0	0.0	18.5	99.9	99.9	n.a.	125.0
SE-02b	87.8	ICDP5059EXOJ001	Lapilli-Tuff	Core	n.a.	100.0	n.a.	n.a.	150.0								
SE-02b	89.2	ICDP5059EXPJ001	Lapilli-Tuff	Core	n.a.	100.0	n.a.	n.a.	107.5								
SE-02b	89.5	ICDP5059EXQJ001	Lapilli-Tuff	Core	n.a.	100.0	n.a.	n.a.	n.a.								
SE-02b	92.6	ICDP5059EXZB701	Lapilli-Tuff	Core	2.0	0.0	56.2	0.1	18.1	1.8	0.3	0.0	21.5	100.0	100.0	n.a.	165.0

SE-02b	97.5	ICDP5059EXRJ001	Lapilli-Tuff	Core	n.a.	100.0	n.a.	n.a.	150.0								
SE-02b	101.5	ICDP5059EX9C701	Lapilli-Tuff	Core	1.5	0.0	58.0	0.4	15.7	2.4	0.9	0.0	21.1	100.0	100.0	n.a.	175.0
SE-02b	106.1	ICDP5059EXSJ001	Lapilli-Tuff	Core	n.a.	100.0	n.a.	n.a.	n.a.								
SE-02b	111.0	ICDP5059EXJC701	Lapilli-Tuff	Core	1.8	0.0	67.5	2.0	10.0	6.5	0.3	0.0	12.0	100.0	100.0	n.a.	160.0
SE-02b	120.8	ICDP5059EXTC701	Lapilli-Tuff	Core	3.4	0.0	68.4	0.4	5.4	6.6	0.0	0.0	15.8	100.0	100.0	n.a.	n.a.
SE-02b	121.4	ICDP5059EXUJ001	Lapilli-Tuff	Core	n.a.	100.0	n.a.	n.a.	n.a.								
SE-02b	128.0	ICDP5059EX3D701	Lapilli-Tuff	Core	1.1	0.0	59.7	0.8	17.8	3.7	0.1	0.0	16.8	100.0	100.0	n.a.	n.a.
SE-02b	134.3	ICDP5059EXVJ001	Lapilli-Tuff	Core	5.4	0.0	60.5	0.8	15.0	3.1	0.0	0.0	15.2	100.0	100.0	n.a.	50.0
SE-02b	138.4	ICDP5059EXDD701	Lapilli-Tuff	Core	3.7	1.2	61.0	2.9	8.6	7.3	0.2	0.0	15.2	98.0	98.5	410.0	32.5
SE-02b	141.5	ICDP5059EXWJ001	Lapilli-Tuff	Core	3.9	16.4	39.2	9.3	1.9	0.0	10.4	0.0	18.9	70.6	75.5	n.a.	0.0
SE-02b	142.6	ICDP5059EXXJ001	Lapilli-Tuff	Core	4.4	48.6	0.0	0.0	0.0	0.0	7.2	1.2	38.6	0.0	0.0	0.0	0.0
SE-02b	144.1	ICDP5059EXYJ001	Lapilli-Tuff	Core	5.3	57.9	0.0	0.0	0.0	0.0	1.0	4.3	31.5	0.0	0.0	0.0	0.0
SE-02b	147.1	ICDP5059EXZJ001	Lapilli-Tuff	Core	10.2	53.3	9.5	0.1	0.1	0.0	1.0	1.0	24.8	15.2	15.5	22.5	0.0
SE-02b	148.7	ICDP5059EXND701	Lapilli-Tuff	Core	7.7	11.3	50.1	9.6	4.1	6.1	0.1	0.0	10.9	81.5	86.0	130.0	0.0
SE-02b	150.3	ICDP5059EX0K001	Lapilli-Tuff	Core	7.5	15.7	46.0	9.9	6.6	3.4	0.3	0.2	10.4	74.6	80.8	170.0	0.0
SE-02b	153.3	ICDP5059EX1K001	Lapilli-Tuff	Core	n.a.	n.a.	n.a.	n.a.									
SE-02b	157.5	ICDP5059EXXD701	Lapilli-Tuff	Core	5.3	0.0	62.6	3.0	10.2	5.6	1.1	0.0	12.3	99.9	99.9	n.a.	45.0
SE-02b	159.0	ICDP5059EX2K001	Lapilli-Tuff	Core	n.a.	n.a.	480.0	25.0									
SE-02b	165.6	ICDP5059EX7E701	Lapilli-Tuff	Core	9.5	0.4	64.0	1.5	6.8	5.0	0.1	0.0	12.7	99.4	99.5	480.0	50.0
SE-02b	168.1	ICDP5059EX3K001	Lapilli-Tuff	Core	n.a.	n.a.	330.0	40.0									
SE-02b	176.1	ICDP5059EXHE701	Lapilli-Tuff	Core	7.2	2.0	66.0	1.3	5.4	4.8	0.6	0.0	12.7	97.1	97.5	n.a.	n.a.

SE-02b	176.4	ICDP5059EX4K001	Lapilli-Tuff	Core	n.a.	340.0	35.0										
SE-02b	177.8	ICDP5059EX5K001	Lapilli-Tuff	Core	8.6	5.1	55.3	1.3	7.0	14.3	0.0	0.0	8.3	91.6	93.9	215.0	20.0
SE-02b	180.9	ICDP5059EXRE701	Lapilli-Tuff	Core	10.5	51.3	0.5	0.0	0.0	0.2	0.0	37.4	1.0	1.0	n.a.	0.0	
SE-02b	181.5	ICDP5059EX6K001	Lapilli-Tuff	Core	n.a.	0.0	n.a.	0.0	0.0								

*Abbreviations: Pl: Plagioclase, Cpx: Clinopyroxene, Ol: Olivine, Sdml: Sideromelane, Pal: Palagonite, Php: Phillipsite, Anl: Analcime, Tb: Tobermorite, Anh: Anhydrite, Gp: Gypsum, n.a.: not analyzed

**Palagonitization extent based on the method used by Pauly et al. (2011), calculated using relative quantities of authigenic phases and primary glass: $(\% \text{Pal} + \% \text{Php} + \% \text{Anl} + \% \text{Tb}) / (\% \text{Sdml} + \% \text{Pal} + \% \text{Php} + \% \text{Anl} + \% \text{Tb}) \cdot 100 \%$